AN ABSTRACT OF THE THESIS OF

Brian Rowbotham for the degree of Master of Science in Environmental Engineering presented on September 18, 2013.

Title: Development of Traceable Metal Oxide Nanoparticles for Examining Environmental Fate and Transport

Abstract approved: _____

Jeffrey A. Nason

The fate and transport of engineered nanoparticles (ENPs) such as titanium dioxide (TiO_2) are of concern due to their increasing use in consumer products. Although analytical methods for detection and quantification of ENPs in environmental matrices are being developed, these methods are difficult, time consuming, and not easily validated for metal oxide ENPs where the metal of interest (e.g., Ti in TiO_2) is abundant in the environment. This work aims to overcome these difficulties by synthesizing TiO_2 nanoparticles "labeled" with rare earth elements. Synthetic conditions will be optimized to create particles consisting of a lanthanum oxide (La_2O_3) core surrounded by a TiO_2 shell. X-ray diffraction, dynamic light scattering, electron microscopy, and zeta potential analysis were used to compare relevant characteristics of synthesized ENPs with unlabeled lab and commercial counterparts. The utilities of labeled particles was then demonstrated using simulated drinking water treatment, an d the ability of labeled particles to be detected against background titanium concentrations shown.

Development of Traceable Metal Oxide Nanoparticles for Examining Environmental Fate and Transport

by
Brian Rowbotham

A THESIS
submitted to
Oregon State University

in partial fulfillment of
the requirements for the
degree of
Master of Science

Presented September 18, 2013
Commencement June 2014

Master of Science thesis of Brian Rowbotham presented on September 18, 2013.

APPROVED:

Major Professor, representing Environmental Engineering

Head of the School of Chemical, Biological, and Environmental Engineering

Dean of the Graduate School

I understand that my thesis will become part of the permanent collection of Oregon State University libraries. My signature below authorizes release of my thesis to any reader upon request.

Brian Rowbotham, Author

ACKNOWLEDGEMENTS

I would first like to thank my advisor Dr. Jeff Nason for allowing me to work on such an exciting and important project. Secondly I would like to thank Peter Esbach, Dr. Mohammed Azizian, Will Young, May Nyman, Dr. Greg Herman, Whitney Schmidt, Dr. Maa=s Subramanian, and any others who helped lend information or equipment to this project. It would not have been possible for me to accomplish this degree without the tremendous support of my friends and family, I am forever grateful. Last but not least is a tremendous thank you to my former roommates and lab mates Chris Durgan, Brian Smith, and Justin Provolt who provided meaningful discussion and relaxation whenever needed.

TABLE OF CONTENTS

TABLE OF CONTENTS (Continued)

Page

TABLE OF CONTENTS (Continued)

LIST OF FIGURES

LIST OF FIGURES (Continued)

Figure Page

LIST OF TABLES

1 Introduction

1.1 Motivation

In the last decade production and use of engineered nanomaterials has drastically increased worldwide and is expected to increase even more dramatically in the coming decades [1, 2]. The dramatic increase of production has led to nanoscale TiO_2 becoming the 3rd most prevalent nanomaterial by number of products [3, 4]. Its widespread use in products such as paint, personal products and photocatalysts has led to nano-TiO_2 being identified in wastewater treatment plants (WWTPs), surface waters, and urban runoff [5-7]. TiO_2 is frequently used as a pigment in food, increasing exposure risks to children [8]. TiO_2 nanoparticles have been shown to have a causal link to Crohn's disease in adults, toxicity to several aquatic species, and inhibit nitrifying bacteria in wastewater treatment plants [9-14]. The toxicity of nano-TiO_2 along with its widespread use has led to the study of its environmental fate and transport. However, high environmental background of titanium makes these studies very difficult and complex [15]. Current methods for separation and quantification of engineered nanomaterials in environmental matrices are complicated, time consuming or still in development. Also, romising techniques in this area do not distinguish between anthropogenic and naturally occurring nanoscale TiO_2, or between several classes of nanoparticles containing the same metal [15]. Detection in environmental matrices is an exciting new field with promising techniques such as Near Infrared Flourescence Spectroscopy (NIRF), single particle ICP-MS, and isotopic or elemental labeling of particles [15-17]. The work described herein aims to further the development of labeled metal oxide nanoparticles as a tool for examining environmental transport and fate using TiO_2 as an initial case study.

1.2 Problem Statement

The creation of a novel material poses many challenges from a synthesis standpoint. Many factors need to be investigated to optimize synthesis of traceable materials to ensure their usefulness as traceable surrogates. These novel materials must have labeling elements with low background concentrations and high sensitivity to instrumental neutron activation analysis

(INAA) while ensuring the particles have the same size, zeta potential, and crystallinity as their commercial counterparts. Elemental labeling of TiO_2 can be achieved by two methods: doping of the TiO_2 crystalline structure with a suitable labeling element, or synthesis of particles with TiO_2 shells surrounding a core containing the labeling element. The former poses problems from a detection standpoint as increasing the dopant fraction increases the limits of detection. Increasing the dopant also increases the amount of dopant on the surface thereby changing its surface properties. As such, a core-shell particle morphology was chosen to pursue the goals of the project however. Little to no previous work has established specific synthesis methods for the particles needed in this study.

1.3 Objective and Hypothesis

The goal of this project was to successfully synthesize core-shell particles consisting of traceable cores with titanium dioxide shells and demonstrate their utility in fate and transport studies. This goal can be divided into 3 objectives:

1) Synthesize and characterize suitable core nanoparticles.
2) Develop procedures for the complete and robust coating of core particles with TiO_2 while ensuring the shell has the same crystalline structure and surface charge as commercially available counterparts.
3) Demonstrate the utility of synthesized core-shell materials in a typical fate and transport study.

1.4 Approach

Objective 1 was accomplished using hydrothermal synthesis of $La(OH)_3$ nanospheres suitable for coating by modifications of a method established by Tang et al.[18]. Synthesis conditions including reagent concentrations, reaction time, and the addition of stabilizing ligands and surfactants were varied and their effects on the resultant materials analyzed. Core particles were characterized by x-ray diffraction (XRD), dynamic light scattering (DLS), zeta potential measurements, small angle x-ray scattering (SAXS) and transmission electron microscopy (TEM).

Objective 2 was met by modifying existing procedures used for the coating of ZnO nanoparticles. Lanthanum hydroxide nanospheres and commercially available lanthanum oxide nanopowder were used in the study of sol-gel nano-coating. Coating of synthesized and commercially available lanthanum materials was performed by sol-gel techniques in ethanol using tetrabutyl orthotitanate (TBOT) and titanium isopropoxide (TTIP) while varying the pH, water concentrations, and core material concentrations to observe effects on coating. Crystalline transformation of the shell material was accomplished through hydrothermal methods as a means of avoiding typical problems associated with high temperature calcination. Coatings were then characterized by XRD, DLS, Zeta potential, SAXS, TEM and energy dispersive X-ray spectroscopy (EDS).

Demonstration of the use of coated particles was achieved by examining the removal of labeled and unlabeled particles in simulated drinking water treatment. Synthesis of true core-shell particles allowed labeled particle removal to be distinguished from background concentrations of TiO_2 in lab-scale setting. Removal efficiencies at different alum doses were examined and quantified using ICP-AES and turbidity measurements.

The remainder of the thesis is organizes as follows: Chapter 2 outlines current production and use of nanomaterials, their detection and fate and transport in the environment, established methods for the synthesis of relevant materials, and typical methods used for nanoparticle characterization. Materials and methods used in this study are discussed in Chapter 3. Results and discussion of synthesis and demonstration of particle utility is presented in Chapter 4. Lastly, conclusions of this study and directions of future work are discussed in Chapter 5.

2 Background

2.1 Production and use

Production and use of engineered nanomaterials has steadily increased worldwide [1]. Because of their increased surface area, nanomaterials are generally more reactive and therefore have unique properties compared to their bulk counterparts and have proven beneficial for incorporation into different products and processes. Currently, engineered nanomaterials are being used for not only electronics, optoelectrics, and cosmetics but they are also used in biomedical, pharmaceutical, energy, environmental, catalytic and material applications [2]. Because of their wide usage and advantages over bulk materials, research has increased over 7 fold from 1995 to 2007 and has continued to increase [2]. Currently, there are over 2100 companies from 48 countries involved in research, manufacturing, or applications of engineered nanomaterials [19]. By 2010 production of these materials reached the order of magnitude of millions of tons per year [1]. Although these materials may be engineered, they also occur naturally in the environment and are created as byproducts in combustion processes such as incineration plants and automobiles [2].

Of the emerging nanomaterials, titanium dioxide (TiO_2) nanoparticles (NPs) have become widely used and produced and are currently the 3rd most prevalent nanomaterial [3, 4]. Although Bulk TiO_2 has many different applications, nearly 70% of it is used in pigments [8]. The bulk TiO_2 industry has historically relied on two manufacturing processes: a sulfate process and a chloride process [4]. The chloride process purifies the TiO_2 containing ore by reacting it a temperatures of 1000°C in a fluidized bed reactor [20]. Because of the nature of this process it is

difficult and expensive to scale. The sulfate method is more complex from a unit operations standpoint. Briefly, the feedstock containing primarily iron and titanium is digested in sulfuric acid followed by the reduction of iron to aid in the separation process. The titanyl sulphate compounds then undergo forced hydrolysis followed by a calcination step to produce crystalline TiO_2 [20]. This process includes numerous byproducts which must be further processed creating complexities and expenses. The sulfate methods has been used for longer than the chloride process; however creates unwanted byproducts and can be expensive while the chloride process is more efficient but expensive to scale up. As the industry has grown, the production costs have increased dramatically. With both methods of production being dated, the bulk TiO_2 industry is poised for a shift to the nanoscale, which would further increase nano-TiO_2 usage and production [4]. Researchers and industry have started using nano-scale TiO_2 in many applications because of its increased photocatalytic and optical properties [8]. In 2005, 2000 tons of nano-TiO_2 was being produced and valued at over $70 million dollars [8]. Of these 2000 tons, nearly 65% was used in personal care products (PCPs) such as sunscreen, lotions, and toothpastes. By 2010, the amount of nano-TiO_2 produced reached 5000 tons and is expected to increase exponentially in the future [4, 8, 21].

There are two major formulations of nano-TiO_2 that are currently manufactured and readily available, P25 and E171. There are multiple manufacturers of E171, a food-grade additive, while the industrially used P25 if manufactured by Degussa Ag. Data on P25 is readily available and has been studied somewhat extensively, yet little is known about the properties of E171 [8]. Though P25 has been studied in greater detail, the usage of E171 dwarfs that of P25 and is very common in PCPs and food products. Usage of nano-TiO_2 in food products has

become more common primarily for its pigmentation properties. Although only a limited number of food products list titanium in the ingredients, concentrations have been found to be as high as 1 μg/mg [8]. Studies have shown that younger children have a much higher exposure to TiO_2 on mg TiO_2/kg bodyweight/day basis because of dietary habits [8]. Nano-TiO_2 is also being used in sunscreens because of its ability to adsorb and reflect ultraviolet radiation while appearing transparent on the skin; as such, usage is expanding rapidly worldwide [19]. Concentrations have been found to be between 0.7 and 5.6 μg/mg in toothpastes, approximately 10 μg/mg in generic brand aspirin, and 14 to 90 μg/mg in sunscreens.

2.2 Fate and Transport

Investigations of the fate and transport of TiO_2 can largely be divided up into field-scale and lab-scale studies. Numerous groups have studied the transport of TiO_2 in the environment via lab-scale work. In simulated wastewater treatment experiments, metal oxide NPs were shown to aggregate in water and be adsorbed to biomass during wastewater treatment; however, only small amounts were found in the effluent [6, 22]. Removal of several different metal oxide nanoparticles in simulated drinking water treatment was examined by Zhang et al. (2008) who found that removal of commercial metal oxide nanoparticles was difficult by normal alum treatment [1]. Column studies have shown TiO_2 NPs can penetrate to significant soil depths, therefore becoming a risk of ground water contamination [23, 24]. Aggregation behavior of TiO_2 has been studied by many groups. It has been shown that TiO_2 NPs largely follow DLVO theory in that increasing ionic strength causes increased aggregation and divalent cations further increase aggregation [25, 26]. Studies have also shown that natural organic matter stabilized

TiO_2 NPs with respect to aggregation and sedimentation, thereby promoting transport downstream [27, 28].

There are far fewer field studies of TiO_2 in the environment due to the increased difficulty of detection highlighted above. Although not definitive, nanoscale TiO_2 has been found to be transported to runoff waters from paint facades by Kaegi et al [7]. Westerhoff and coworkers have shown that TiO_2 NPs entering full scale WWTPs are removed at above a 95% efficiency, though TiO_2 NPs were found in the effluent of all 10 plants studied [29]. This removal indicates that most NPs will be captured in the activated sludge, which is often applied to the land. A study done by Saiers et al. (2003) used TiO_2 as a tracer to test transport of suspended particles in the Florida everglades [30]. The study was made possible by very low background concentrations of titanium. Significant downstream transport of the materials occurred due to the fact that adsorption of the TiO_2 onto natural sediments did not occur due to the small size of the particles.

Current studies of environmental fate and transport of TiO_2 either rely on lab-scale procedures where background concentrations are not of concern or require complex separation techniques such as field flow fractionation, filtering, or imaging which are incredibly difficult or require specialized equipment. These techniques also do not discern between anthropogenic and naturally occurring nanoscale colloids. A limited number of studies have used isotopically labeled ZnO nanoparticles as an effective means of studying uptake in biota [16, 31] against high background concentrations. Von der Kammer et al. (2012) has called for the need of labeled particles for the study of environmental fate and transport for elements having high background concentrations in the environment such as Ce and Ti [15].

2.3 Toxicity

Though TiO_2 poses less of a toxicity threat than many other emerging nanomaterials, toxic effects have been observed. Toxicity studies have been performed on organisms ranging from aquatic species and mammalian rodents to bacteria and mammalian cells. Though the findings are somewhat inconsistent between studies, nanoscale TiO_2 has been shown to have varying toxic effects resulting from several different mechanisms of toxicity.

Toxicity of ingested and inhaled TiO_2 NPs has recently been studied with results concluding that inhalation has major toxic effects. Ultrafine particles are retained in the lungs for much longer periods of time than their bulk counterparts. Secondly, ultrafine particles produce more oxidative stress causing greater inflammation [10]. Ferin and Oberdorster showed that ultrafine TiO_2 deposited itself in different parts of the lung upon inhalation causing both longer retention and greater inflammation in rats [32]. TiO_2 has been specifically studied for inhalation toxicity in many rodents. Inhalation of TiO_2 NPs was shown to cause lung inflammation in mice and rats, but not hamsters [33]. Rats in this study showed the formation of lung lesions at mid and high doses.

Bacterial populations are some of the most susceptible groups to nanoscale toxicity. Pagnout et al. showed the effect of pH on interactions between *E. coli* and TiO_2 NPs [34]. At pH values where bacteria cells and NPs were oppositely charged, toxicity increased. Zheng et al. showed that Nano-TiO_2 inhibits nitrifying bacteria in WWTPs over long periods of time (70 days) by reducing the bacterial diversity in the activated sludge system [11].

Gottschalk et al. modeled environmental release of TiO_2 and other nanomaterials and showed that surface water release is the most likely scenario for TiO_2. Possible contamination of

surface waters highlights the need for the study of toxicity of TiO_2 on aquatic species. Federici et al. showed that exposure to TiO_2 suspensions, although not lethal, caused respiratory distress and other sub-lethal toxicity in rainbow trout [12]. TiO_2 has also been shown to have more dramatic effects on other species. In a study by Ates et al., TiO_2 aggregates were shown to accumulate in *Artemia salina*, a species of brine shrimp, causing mortality for 14% of adults [13]. A study done on crustaceans by Heinlaan et al showed TiO_2 to have no toxic effects on *T. platyrus,* but induced 60% mortality in *D. magnia* [14]. Initial tests by this group showed higher toxic effects for illuminated TiO_2 NPs.

TiO_2 NPs are used mainly for their strong photocatalytic properties which also pose a significant toxicity threat. Under ultraviolet light these particles can create reactive oxygen species (ROS), causing photocytoxicity. There are a large number of studies showing that nanoscale TiO_2 generates significantly more ROS than its bulk counterpart when compared on a mass basis [35-38]. In a study by Li et al., the concentration of ROS was directly related to toxicity to *E. coli*, showing nano-TiO_2 to be much more toxic [35]. Dunford et al. isolated nanoscale TiO_2 from sunscreens and found that hydroxyl radicals generated by the TiO_2 caused oxidative damage to both human DNA in vitro and in human fibroblasts [36]. ROS production by TiO_2 NPs was shown to significantly inhibit growth rates in phytoplankton [37]. The results of this study are noteworthy because in sea water the high ionic strength induces nanoparticle instability which can be related to lower toxicity.

As engineered nanomaterials are synthesized specifically to have unique properties compared to their bulk counterparts, concern has arisen about their possible toxic effects. Bacterial populations can be greatly affected by nanoscale TiO_2, while toxic effects on aquatic

life vary among species. In human's TiO_2 has been shown to cause DNA damage and inflammation of the intestines which can cause diseases like Crohn's in adult life. The studies discussed were primarily undertaken at concentrations much higher than currently seen in the environment. In the future however, increasing production of nanomaterials could see these concentrations studied approached. Though non-lethal in most cases TiO_2 has been shown to be a concern from a toxicity standpoint thereby putting a demand on the study of its fate and transport in the environment.

2.4 Detection of ENPs

Assessment of the fate of engineered nanomaterials in the environment poses many difficulties. Typical analytical methods used to quantify and characterize ENPs must be modified or abandoned all together when applied to ENP detection in environmental matrices. As an emerging field of technology, expected concentrations of engineered nanomaterials in the environment are still relatively unknown and expected to change rapidly in the coming decades. Probabilistic models using material flows to assess concentrations of many engineered nanomaterials have been developed. A model by Gottschalk et al. estimated concentrations to be in the ng-µg/kg range for soils, sludges and sediments, ng/L range in surface waters and in the pg/m^3 range for air [39]. Similar models have been created and used for risk assessment, also suggesting environmental concentrations of nano-TiO_2 to be in the range ng-µg/L of water or kg of soil and much lower for concentrations in air [40]. The low levels of these materials in environmental matrices are one of the biggest challenges in understanding their role in the environment [39]. Tools such as inductively coupled plasma mass-spectrometry have the

ability to detect nanoparticle concentrations in this range, but have other drawbacks and only provide a small part of the overall picture [15].

Secondly, techniques must be able to avoid interference of natural nanoparticles in environmental matrices [41]. Separation techniques such as centrifugation exist and can be used, but can alter the physic-chemical state of particles [41] and induce aggregation [42]. Not only do other nano-scale particles exist in environmental matrices, but metal oxides and other materials or minerals containing the metal of interest (e.g., Ti) may occur naturally. Titanium, for instance, is the 9th most abundant element in the earth's crust and concentrations in soils range from 0.3 to 6% and from 0.1 to 18 μg/L in freshwaters [15]. TiO_2 occurs naturally in the mineral forms ilmenite, brookite, anatase, and rutile [43]. These minerals can occur both on the bulk scale and nanoscale, making detection of engineered TiO_2 NPs difficult on two fronts. One must distinguish between anthropogenic and natural materials and also nano and bulk materials. Detection of metal oxide ENPs in environmental matrices is also made incredibly difficult by the abundance of ENPs being far less than that of background concentrations [44]. Environmental matrices containing metal oxides are complicated furthermore by the fact that ionic forms of the metal elements adsorb strongly to natural occurring surfaces [15].

Electron microscopy is currently a predominant technique used to analyze the presence and composition of ENPs. This technique can provide information on the presence, location and composition of ENPs [15, 45]. High-resolution Transmission Electron Microscopy (TEM) and Scanning Electron Microscopy (SEM) can provide the needed resolution to examine samples down to a scale of several nanometers [15, 46]. TEM uses electrons transmitted through the specimen to provide a detailed image [46]. Because the electrons are being transmitted through

the sample, specimens need to be thin, making larger particles or aggregates harder to image. In SEM, a beam of electrons is produced and focused on the specimen. Electrons scattered by the specimen provide a detailed picture of the surface [46]. Energy-dispersive X-ray spectrometry (EDS) is often paired with electron microscopy. This technique provides elemental analysis of samples by X-ray excitation. EDS, when used quantitatively, has approximately 20% uncertainty [46]. EDS could be used to discern between natural and anthropogenic materials based on the recognition of impurities and naturally occurring accompanying elements, but can be difficult based on the low sensitivity of the technique [15]. Electron energy loss spectroscopy (EELS) can also be paired with TEM to provide another method of elemental analysis with uncertainties around 10% [46]. Neither EDS nor EELS provide information on crystalline structure, an important property that can determine relevant parameters effecting how an ENP will act in the environment. Selected Area Electron Diffraction (SAED) can be paired with TEM to provide such details on crystalline properties [46]. Sample preparation for electron microscopy can be complicated and has many drawbacks. Standard TEM and SEM samples must be placed in an ultra-high vacuum preventing the use of wet samples [46]. Samples must also be prepared and dehydrated properly which can lead to disturbance of the sample [46, 47]. SEM samples must be coated with a thin layer of Au, Pt, or C to keep the samples conductive and to keep them grounded to prevent charge buildup on the specimen surface. This disturbance of samples by coating is problematic when looking at environmental samples and may create artifact particles or aggregation that may confuse the viewer [15, 47]. Though SEM and TEM can be used to discern between anthropogenic and natural NPs by identifying structures, surface

coatings, etc. there is no direct way to discern between the two classes and another technique must be used to distinguish between the two [15].

Characterization and detection of metallic nanoparticles is commonly achieved with inductively coupled plasma mass spectrometry (ICP-MS). Mass spectrometry usually consists of a mass analyzer, a detector system, and an ion source [46]. ICP-MS can provide a high level of detection needed for environmental samples. ICP-MS provides a relatively quick and easy measurement of metal concentrations. In some cases, detection limits can be in the parts per trillion range. ICP-MS can be paired with many different separation techniques to provide a more complete characterization of samples containing ENPs.

By coupling a separation technique with ICP-MS, elemental concentrations of each size fraction can be determined [48]. The most popular separation technique has become Field Flow Fraction (FFF). This method works by applying a laminar flow through a narrow channel coupled with an orthogonal force field resulting in lower velocities for larger particles and size separation at the outlet [48]. FFF can exist in many different forms with the two most common being flow field FFF and gravity field FFF, with the techniques separating by hydrodynamic radius and buoyant mass respectively [48]. Hydrodynamic chromatography (HDC) is another common physical separation technique that has recently been applied to ENPs coupled with ICP-MS [48, 49]. Briefly, samples are passed through columns of inert material such as silica causing larger particles to travel faster through the column due to their higher average velocity [50]. Lastly, capillary electrophoresis (CE) has been applied to the separation of nanomaterials based on electrophoretic mobility [48, 51, 52]. Though relatively fast compared to other techniques, data interpretation can be complicated [52]. These coupled techniques have several

drawbacks. They only give estimates of size distribution and not sizing info on individual particles. They also cannot discern between particles with the same size containing different concentrations of the analyte in question [48].

Although ICP-MS typically only provides total metal concentrations, in recent studies ICP-MS operated in single-particle mode has been used to gain data on the size of ENPs as well [15, 17, 53-55]. In this technique, samples are not acid digested and individual particles are allowed to pass through the plasma. The intensity readings of each particle are collected as a function of time. Pulse height and pulse distributions are then correlated with NP size and number concentration respectively [15, 17, 53-55]. Though accurate, this procedure is very intensive and requires extensive calibration. Discerning between dissolved metals and NP pulses is also a complicated task [54] . Although SP-ICP-MS is a promising technique for analysis of ENPs, it is still very new and under development [15]. SP-ICP-MS uses the assumption that particles are spherical when calculating size. Initial work using the technique also focused on monodisperse samples. In a recent study, the technique was used to examine Ag nanowires, TiO_2, and ZnO with polydisperse size distributions [17]. Another drawback to SP-ICP-MS is that it is currently best suited for analysis of one metal at a time [53, 55]. Many environmental samples might have several analytes of concern. This problem may be overcome by pairing SP-ICP-MS with asymmetrical Field Flow Fraction (AF4). This technique could provide data on size, detection, and compositional analysis at a detection level of parts per billion [54].

Another new technique to emerge for the detection and analysis of ENPs is the use of Instrumental Neutron Activation Analysis (INAA). This technique renders ENPs radioactive by neutron activation, which can then be detected by using gamma spectrometry. Individual

elements emit different gamma rays so individual elements can easily be analyzed. In a preliminary study by Oughton et al. this technique has been shown to provide great accuracy in detection of ENPs in environmental samples. Detection limits can be as low as part per billion [56]. One of the biggest advantages to this technique is the ability to detect ENPs in dirty matrices [57]. Samples can therefore be analyzed without complicated separation techniques or disturbance of the ENPs. This technique does have some drawbacks; only certain elements have suitable neutron absorption cross-sections [57]. Because of this limitation, the idea of labeling ENPs with suitable elements for INAA has been introduced and recently proven to provide great detail on ENPs in complicated matrices [57]. This technique also renders samples radioactive so they would not be available for use in other methods.

2.5 Synthesis Methods

Nanomaterials specifically labeled for the study of environmental fate and transport could be synthesized by one of many methods. It would be advantageous to synthesize these materials in regards to high sensitivity to INAA (Table 2-1) and low background concentrations.

Table 2-1. Suitable labeling elements with INAA sensitivity [58].

Sensitivity (picograms)	Elements
1	Dy, Eu
1–10	In, Lu, Mn
10–100	Au, Ho, Ir, Re, Sm, W
100–1000	Ag, Ar, As, Br, Cl, Co, Cs, Cu, Er, Ga, Hf, I, La, Sb, Sc, Se, Ta, Tb, Th, Tm, U, V, Yb
1000–10^4	Al, Ba, Cd, Ce, Cr, Hg, Kr, Gd, Ge, Mo, Na, Nd, Ni, Os, Pd, Rb, Rh, Ru, Sr, Te, Zn, Zr
10^4–10^5	Bi, Ca, K, Mg, P, Pt, Si, Sn, Ti, Tl, Xe, Y
10^5–10^6	F, Fe, Nb, Ne
10^7	Pb, S

Among those elements listed in Table 2-1 Eu, Au, Hf, La, Ce, and Sc [59] all have high sensitivity to INAA and suitably low background concentrations, making them appropriate for elemental labeling.

Two methods of labeling NPs with other elements suitable for these studies exist: doping of the TiO_2 crystal lattice with a suitable labeling element or synthesizing core-shell particles consisting of a core containing the labeling element and a TiO_2 shell. The disadvantage of doping particles lies in the fact that as dopant fraction increases, thereby increasing detectability, the surface properties of the materials are affected, making the labeled particles potentially unsuitable surrogates for their undoped-counterparts. Core-shell composite particles, however, could potentially be labeled with a high fraction of labeling element while still retaining the surface properties of TiO_2.

A plethora of synthesis techniques exist for the creation of metal oxide nanoparticles, doped metal oxide nanoparticles, and core-shell nanoparticles. Metal oxide nanoparticles including TiO_2 and lanthanide nanoparticles have been synthesized in numerous studies by complicated processes such as flame combustion, multi-step precipitation, chemical vapor deposition and mechanochemical methods [60-64]. Although these methods yield nano-sized particles, the synthesis processes are complicated and the resulting particles are often highly aggregated. More promising methods include sol-gel and hydrothermal methods. Metal oxide nanoparticles have been synthesized by a number of groups using these methods [18, 65-70]. Briefly, sol-gel processes involve a sol, a stable suspension of colloidal solid particles within a liquid, created by the reaction of an appropriate precursor [71]. Well defined crystallinity in

samples created from sol-gel processes is usually achieved by a calcination step in which the samples are dried and heated at very high temperatures. Calcination can lead to significant particle aggregation [67]. Hydrothermal synthesis overcomes this obstacle by forcing crystal growth at high vapor pressures in aqueous solutions at relatively low temperatures. Synthesis of rare-earth doped TiO_2 has been achieved by sol-gel procedures where titanium precursors are hydrolyzed in the presence of rare-earth salts [72-74]. These techniques are relatively straightforward but would not provide identical surface charges to their undoped counterparts. Core-shell structures, however, should provide useful surrogates for unlabeled counterparts and have been synthesized by methods such as chemical vapor deposition, one step hydrothermal synthesis, and sol-gel processing [65, 70, 75-78]. Chemical vapor deposition requires the use of specialized equipment and is hard to accomplish for individual particles, while one-step synthesis procedures often creates odd morphology. Sol-gel nanocoating, however, is a well-studied and relatively simple technique for the synthesis of core-shell structures.

Sol-gel coating usually involves a metal containing precursor, often an alkoxide, that undergoes hydrolysis and condensation of the precursor in the following reaction [69].

Hydrolysis:

$$M(OR)_4 + H_2O \rightarrow M(OH)_4 + 4ROH$$

Condensation:

$$M(OH)_4 \rightarrow MO_2 \cdot xH_2O + (2\text{-}x)H_2O$$

Coating can be achieved by the homogeneous nucleation of primary TiO_2 particles which then coat the surface of oppositely charged core particles such as SiO_2 [79]. This technique however, can only be performed at pHs where particles are oppositely charged. These conditions often

occur at very acid pH and can only be used for extremely corrosion resistant particles like silica. Sol-gel coating can also be achieved by the heterogeneous nucleation of precursor molecules on the solid substrate of the core material. To ensure heterogeneous nucleation, care must be taken to ensure the reaction proceeds slow enough by carefully controlling reaction conditions such as temperature and reactant concentrations.

By carefully controlling the amount of water in solution, hydrolysis can be slowed down and careful coating of the core material achieved, as demonstrated in studies by Ocana and Demirors [70, 76, 80]. Using different precursors, either other titanium alkoxides or titanium containing salts change the speed of the titanium reaction [65, 77, 78, 81, 82].

The synthesis of suitable core nanoparticles for sol-gel nanocoating can be achieved by simple hydrothermal methods. This method has been used to create various Lanthanum nanorods and nanospheres with controlled morphology [18, 68, 83]. Reactions times and temperatures in these studies had a key impact on crystallite sizes, while morphology of these particles was also controlled by use of different reagents and reagent concentrations forcing desired crystal growth. It is important to note that this method still needs to be paired with calcination to create La_2O_3.

2.6 Characterization

As discussed in previous sections, the fate and transport of nanomaterials in the environment is dependent on size, morphology, surface charge, crystalline structure, etc. Materials synthesized for use in fate and transport studies must, therefore, be characterized with these properties in mind. Aggregation state and particle size has been shown to have a controlling effect on environmental fate and transport [25, 30]. Dynamic Light Scattering (DLS)

has been used not only to determine particle size in metal oxides, but to determine aggregation behavior [69, 84]. One possible drawback of using DLS for size determination is its poor ability to handle polydisperse suspensions. The nature of DLS is such that scattering intensities are proportional to diameter raised to the 6^{th} power [85], skewing results if larger aggregates are found in solution. In a study by Domingos et al. (2009), the need for complementary analysis techniques was highlighted [47]. Nanoparticle size and morphology has also been determined by small angle x-ray scattering (SAXS) [86]. Size results from these two methods can then be compared to TEM images, which have been used extensively to study numerous classes of nanoparticles including metal oxides with core-shell structures [69, 70, 76, 80, 87].

TiO_2 has been shown to follow DLVO theory [1, 25, 27], warranting the need for characterization of surface charge of synthesized materials. Zeta potential measurements have been performed on numerous metal oxide materials to give a better understanding of how they will act in the environment [1, 19, 88]. To serve as surrogates in fate and transport studies, labeled particles must then have surface charge identical to their unlabeled counterparts. Liao et al. [76] showed that titania coated zinc oxide nanoparticles took the zeta potential of the amorphous titanium dioxide coating, proving zeta potential measurements can be used as a technique for confirming the coating of nanomaterials.

The surface charge and aggregation behavior of TiO_2 varies with different fractions of the crystal structures consisting of anatase and rutile [89]. Differences between crystal structures in core and shell materials can also greatly affect the success of synthesizing core-shell structures [65]. X-ray diffraction (XRD) has been used routinely to characterize the crystal structure of commercial and lab-synthesized metal oxides including TiO_2 [16, 18, 19, 67, 87]. Another

advantage of this technique is the ability to determine crystallite size particles by the Scherrer equation as follows:

$$D = \frac{K\lambda}{\beta \cos\theta}$$

Where:

D is the crystallite size

λ is the X-ray wavelength

K is the crystallite shape constant (usually 0.89)

B is the full width of the diffraction peak at half max

θ is the diffraction angle

This method has been used to determine particle size in various lanthanum oxide and hydroxide structures, as well as titanium dioxide [18, 90]. Crystal structure can also be determined by selected area electron diffraction (SAED) using TEM. Use of TEM to determine crystal structure has drawbacks including high expense, sample destruction, and more complicated sample preparation when compared to XRD.

3 Materials and Methods

3.1 Materials Characterization

3.1.1 Transmission Electron Microscopy

Particle size and morphology was studied via Transmission Electron Microscopy (TEM) (FEI Titan 80-200 TEM/STEM). Prior to TEM imaging, particles were dispersed in 100% ACS/USP Grade Ethanol. After dispersion in ethanol particles were placed in a sonic bath (VWR B1500A-MTH) for 30 minutes. 5 μL was pipetted onto Ted Pella TEM grids (Formvar/Carbon 400 Mesh) and left to air dry for 30 minutes prior to storing for imaging.

Particle morphology was imaged and studied in TEM mode while chemical mapping was done in Scanning Transmission Electron Microscope (STEM) mode via Energy-dispersive X-ray Spectroscopy (EDS) utilizing a High Angular Dark Field Detector (HAADF) and 4 embedded Bruker Silicon Drift Detectors (SDD). Chemical maps were created using the SDDs and analyzed in Bruker Esprit software.

Initial coating was also confirmed via an FIB lift-out to examine a cross section of a typical particle aggregate. This complicated technique was performed by locating a suitable particle aggregate using Scanning Electron Microscopy (SEM) (FEI Quanta 3D dual beam SEM/FIB). A protective layer of Tungsten was applied using the Focused Ion Beam (FIB) and the FIB was then used to cut out a cross section of sample 50 to 120 nm thick and removed using a glass needle. The cross section was then attached to a TEM grid and analyzed using Energy Filtered Transmission Electron Microscopy (EFTEM) (FEI Titan 80-200 TEM/STEM) and EDS.

3.1.2 X-Ray Diffraction

Crystal structure of synthesized and purchased nanomaterials was studied using X-Ray Diffraction (XRD) (Bruker-AXS D8 Discovery, Madison, WI) with a Cu X-ray source. Scans were typically performed between 20° and 80° at a rate of 5°/min. Samples were prepared by centrifuging particle solutions, decanting the supernatant, collecting the pellet, and drying in an oven at 80°C. After drying, particles were ground with a mortar and pestle and small amounts

placed on a circular glass slide attached to a Bruker 25mm specimen ring with modeling clay (amorphous). A small amount of ethanol was added and after drying the mixture was pressed flat with a microscope slide. Care was taken to ensure the level of the sample was even with the sample holder edge so as to not interfere with measurements. After background subtraction, XRD patterns were compared to common crystallographic indices.

3.1.3 Small Angle X-Ray Scattering

Particle size was studied using an Anton Paar SAXSess mc^2 Small X-Ray Scattering instrument. Particle dispersions were sonicated for 30 minutes in a Sonics VCX 500 Watt Sonicator unit with a high intensity cup-horn prior to analysis. Sonicated dispersions were added to 1.5 mm glass capillary tubes purchased from Hampton Research (Glass no. 50) and sealed using a blow torch prior to SAXS analysis. Scattering curves were created for DDI water to determine background scattering prior to use of each different capillary tube.

3.1.4 Metals Concentrations

After synthesis, metals concentrations were measured using Inductively Coupled Plasma Atomic Emission Spectroscopy (ICP-AES) (Varian Inc. Liberty 150) to investigate the extent to which synthesis reactions occurred. Prior to analysis, particles were suspended in a 5% nitric acid solution (Aristar Ultra, 67-70%) and allowed to digest for 30 minutes before running through the instrument without any filtering.

3.1.5 Nitric Acid Stability Test

To probe the possibility of core-shell morphology, a method was developed from Hirakawa and Kamat [91] to test the stability of synthesized particles in nitric acid. Particle were suspended in a 5% nitric acid solution (Aristar Ultra, 67-70%) and filtered either immediately or after 5 minutes of exposure to the acid solution using 0.02 μm inorganic membrane syringe filters. Concentrations of titanium and lanthanum in the filtrate were then measured by ICP-AES.

3.1.6 Dynamic Light Scattering

Particle size and size distributions were quantified using Dynamic Light Scattering (DLS) (90 Plus Particle Size Analyzer, Brookhaven Instruments, Holtsville, NY). Prior to dilution into polystyrene cuvettes, solutions were sonicated for 30 minutes in a Sonics VCX 500 Watt Sonicator unit with a high intensity cup-horn at 49% power with a circulating ice bath and an 8 seconds on, 4 seconds off pulse setting. Typical measurements were performed at 10 ppm and done in triplicate.

3.1.7 Zeta Potential Measurements

Zeta potential (ζ) of purchased and synthesized particles were measured and used as a means of evaluating the coating of synthesized material. Measurements were performed on a Brookhaven ZetaPALS instrument (Holtsville, NY). Electrophoretic mobility measurements consisted of 5 runs utilizing 20 cycles per run. Measurements were made in 1 mM KCl at pH values ranging from 3 to 11. Zeta potential was calculated from the electrophoretic mobility using the Smoluchowski equation.

3.2 Materials Synthesis and Characterization

3.2.1 Commercial La_2O_3 Nanopowder

Initial coating experiments were performed using commercially available La_2O_3 nanopowder purchased from Sigma Aldrich (Lanthanum(III) Oxide Nanopowder <100nm particle size). Prior to coating experiments, particles were dispersed into either distilled deionized water (DDI) with a resistivity of 18.2 MΩ·cm (ELGA PureLab Ultra), 100% ACS/USP Grade Ethanol, or a mixture of both solvents and sonicated for 30 minutes using a Branson Digital 450 Sonifier unit equipped with a high-power disruptor horn set at 50% power utilizing a 10 second on/5 second off pulse while cooled using an ice bath.

3.2.2 Synthesis and Characterization of $La(OH)_3$ Nanospheres

$La(OH)_3$ nanospheres were synthesized using a modification of a hydrothermal method by Tang et al. [18]. 1 mmol $La(NO_3)_3 \cdot 6H_2O$ (Alfa Aesar, 99.9%) and 2 mmol ACS Grade Citric

Acid (Sigma Aldrich, >99.5%) was dissolved in 20mL DDI water. 10 ml of a 10% by volume KOH solution was then added to the first solution, and stirred briefly. Telfon-lined Parr acid digestion vessels were filled to 66% of their total volume, modified from 80% of their total volume in the original cited procedure. Vessels were treated at 180°C for 12 hours in a Yamata DX400 convection oven. After cooling, the solution was transferred to a 50 mL polyethylene centrifuge tube and centrifuged at 5000G for 30 minutes. After decanting the supernatant, the pellet was re-suspended in DDI water, sonicated for 15 minutes in a VWR B1500A-MTH sonic bath set to high power. This washing/rinsing procedure was repeated twice to ensure the solution had a conductivity of ≤ 5 μS/cm. The effects of the surfactants added during synthesis were probed by adding either Cetyltrimethylammonium Bromide (CTAB) or Triton X100, both purchased from Sigma Aldrich, to several synthesis trials.

3.2.3 Coating of Commercial La_2O_3

Initial coating of commercially available La_2O_3 particles was accomplished using a sol-gel method modified from Liao et al [76]. 0.3264 g of La_2O_3 nanopowder (Sigma Aldrich) was added to a solution containing 90 mL 100% ACS/USP Grade Ethanol and 9 mL of ACS grade NH_4OH (Fischer Scientific, 28-30%) and sonicated for 30 minutes using a Branson Digital 450 Sonifier unit equipped with a high power disruptor horn for 30 minutes at 49% power and a pulse setting of 10 seconds on, 5 seconds off. A second solution containing 0.4 mL reagent grade tetrabutyl orthotitanate (TBOT, 97%, Sigma Aldrich) and 7.1 mL of DDI water was sonicated for 10 minutes in a VWR B1500A-MTH sonic bath set to high power and added at 2 mL/min using a New Era syringe pump (NE-300, Wantagh, NY). pH of the initial solution was varied by eliminating NH_4OH from the La_2O_3 suspension or adding ACS grade HCl prior to adding the secondary TBOT containing solution. Upon addition of the TBOT precursor solution, the solution was stirred for 3 hours and the precipitated solids collected by centrifugation at 5000G for 30 minutes. Following centrifugation, the supernatant was decanted and the particles resuspended in 100% ACS/USP Grade Ethanol. This washing and rinsing procedure was repeated once with ethanol to ensure no more hydrolysis of the TBOT occurred and then rinsed

in the same fashion 3 times using DDI water. Coated particles were characterized via TEM, DLS, XRD, and zeta potential measurements.

TBOT is known to be highly reactive in the presence of water and the effects of water concentrations on the coating of La_2O_3 nanopowders were studied using a modified procedure from Ocana et al. [70]. Varying amounts of La_2O_3 nanopowder was dispersed into a solution containing either 0.22 or 0.44 mL of DDI water and an aliquot of 100% ACS/USP Grade Ethanol to bring the total volume to 25 mL. This solution was sonicated and a secondary solution containing 0.237 mL reagent grade TBOT (Sigma Aldrich, 97%) and 4.763 mL100% ACS/USP Grade Ethanol was added after 5 minutes of bath sonication. The solution was then stirred for 3 hours and washed and rinsed using the same procedure as initial coating experiments described above. Particles were characterized by DLS, TEM, XRD and zeta potential measurements.

3.2.4 Coating of synthesized $La(OH)_3$ Nanospheres

Coating of $La(OH)_3$ nanospheres was performed using a procedure modified from Ocana et al. [70]. The amount of water contained in the primary Ethanol/$La(OH)_3$ solution was varied between 0, 0.27 and 0.54M and the concentration of $La(OH)_3$ nanospheres varied between 100 and 500 mg/L. Experiments were also performed using this procedure, but synthesis was performed in 30 mL glass vials sealed with polystyrene caps and heated in an oven at 100°C for 3 hours. Four conditions were examined: two samples were performed using TBOT as a precursor with 0.0M and 0.54M water concentrations and 2 samples were coating using titanium isopropoxide (TTIP) purchased from Alfa-Aesar under identical water concentrations. Precipitated solids were washed and rinsed using the procedure described above and characterized by DLS, TEM, zeta potential measurements, and stability to dissolution in 5% nitric acid.

3.2.5 Hydrothermal treatment of coated material

The coating procedures outline above have been shown to create an amorphous TiO_2 coating [70, 76]. To properly use core-shell materials as a surrogate for available TiO_2 this amorphous coating must undergo thermal treatment to form a crystalline material. Treatment of coated particles was done by transferring 16.67 mL of washed and rinsed coated material to a

Parr acid digestion vessel with a Teflon liner and hydrothermally treated at 220°C for 12 hours. Crystallinity was verified by XRD, the particle size was compared to untreated material using DLS, and changes in surface charge were quantified using zeta potential measurements.

3.3 Examination of removal during simulated drinking water treatment

The removal efficiency of synthesized particles in simulated drinking water treatment was examined using jar testing. Water used for the study was taken from the influent to Corvallis's H.D. Taylor water treatment plant. pH as reported by the facility was 8.1 upon collection. Sample water was filtered using a Quickfilter® polyethersulfone membrane filter (QED, Ann Arbor, MI). Six 2L B-KER^2 polystyrene jars (Phipps & Bird) were used for testing. 1 L of filtered plant influent was added to each jar. Particles were added at approximately 12.5 mg/L (total particle weight) and rapidly mixed for a brief period followed by sampling of the water. Initial samples were analyzed for metals concentration using ICP-AES and turbidity measurements were taken by a Hach 2100P turbidity meter. A stock solution of alum was created by dissolving ACS grade aluminum sulfate hydrate purchased from EMD Millipore into DDI water. Different amounts of the stock alum concentrations were added to create alum concentrations of 0 to 30 mg/L. Suspensions were mixed at 120 rpm for 2 minutes, followed by mixing at 20 rpm for 20 minutes using a typical jar testing apparatus. Finally, paddles were removed and suspensions were allowed to settle for 1 hour. After settling, pH was measured and samples were taken and measured for metals concentration and turbidity. 3 tests were undertaken: one using 12.5 mg/L of $La(OH)_3@TiO_2$ particles, one using 12.5 mg/L synthesized TiO_2 particles, and one mixed system of 12.5 mg/L core-shell particles and 12.5 mg/L titanium particles. Prior to jar testing, both $La(OH)_3@TiO_2$ and TiO_2 particles were analyzed by DLS, Zeta Potential, and XRD.

4 Results and Discussion

4.1 Characterization of Commercial La_2O_3 Nanopowder

Prior to coating experiments, lanthanum oxide core particles were dispersed in water via ultrasound and size was studied using DLS. Because of the effect of possible large aggregates, measurements are reported with and without a built-in numerical dust filter. Hydrodynamic diameter was measured in triplicate and reported in Table 4-1. After 30 minutes of high-power sonication, dispersions of the nanopowder still contained large aggregates as shown by the difference in hydrodynamic diameters with and without the numeric dust filter. Samples were very polydisperse with sizes much greater than those reported by the manufacturer (>100 nm).

Table 4-1. DLS measurements on La_2O_3 nanopowder

	With numerical dust filter		**Without numerical dust filter**	
Sample	Hydrodynamic Diameter (nm)	Polydispersity	Hydrodynamic Diameter (nm)	Polydispersity
1	400.1	0.3	655.9	0.356
2	407.9	0.323	742.9	0.363
3	371.2	0.288	393.9	0.302

Zeta potential was measured from pH 3 to 11 and is reported in Figure 4-1. The isoelectric point (IEP) for the purchased nanopowder is approximately 9-9.5. Reported values for the IEP of La_2O_3 are between 9.5 and 10.5 [92], indicating our powder is not purely oxide. It is also important to note that at a neutral pH of 7, the ZP measures +33.7 mV, indicating moderate stability of particle suspensions near neutral pH values.

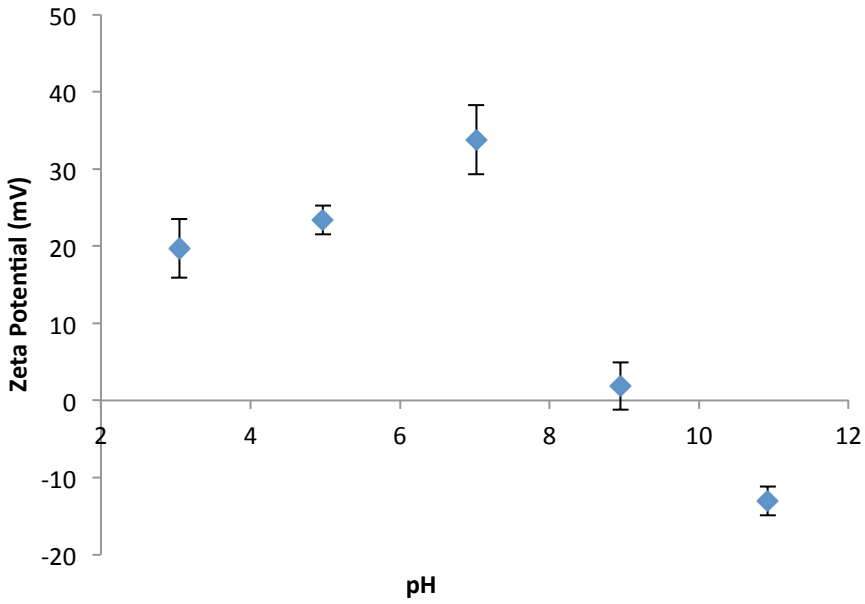

Figure 4-1. Zeta potential pH titration of commercial La_2O_3 nanopowder in 1 mM KCl

TEM imaging was used to study the morphology of the purchased nanopowder prior to coating with TiO_2. Dispersions of the nanopowder consist of large particle aggregates with a wide distribution in sizes ranging from less than 100 nm to over 1µm. Initial laboratory experiments to attempt to synthesize La_2O_3 nanopowders resulted in similar morphology and can be found in the Appendix. The formation of the oxide phase only occurs at 750°C and above [67], but care must be taken when calcining. Significant sintering of materials can occur at temperatures as low as 850°C, causing significant particle aggregation like that shown in Figure 4-2.

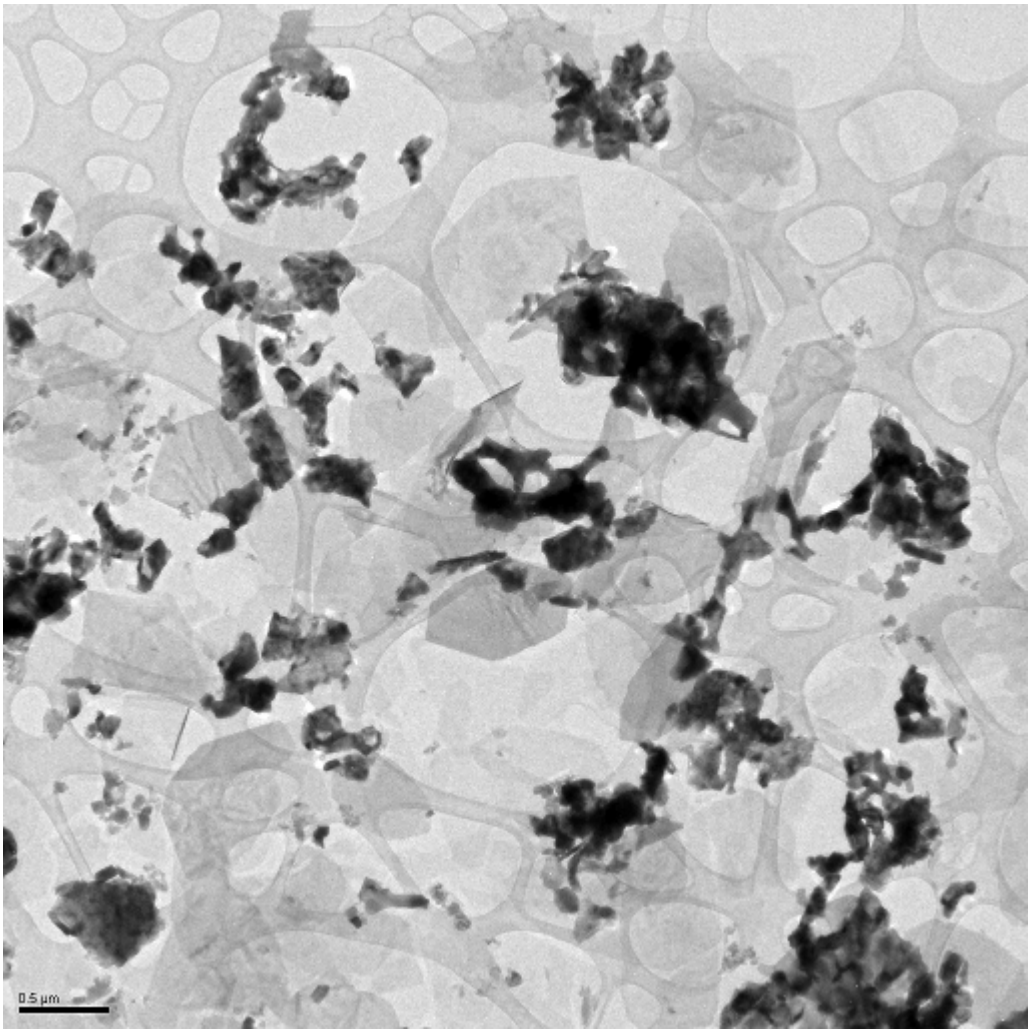

Figure 4-2. TEM Image of commercial La_2O_3 nanopowder dispersion.

Lastly, crystal structure of the purchased nanopowder was studied by XRD. The resultant XRD pattern of the material is shown in Figure 4-3. Several phases exist besides the hexagonal La_2O_3 structure. $La(OH)_3$ and $La(HCOO)_3$ are both clearly present. Rare earth oxides, lanthanum oxide in particular, has been shown to undergo nearly complete hydroxylation within 24 hrs when exposed to atmospheric water vapor [93]. Because materials were not kept in a glove box, hydroxylation of the nanopowder most likely occurred.

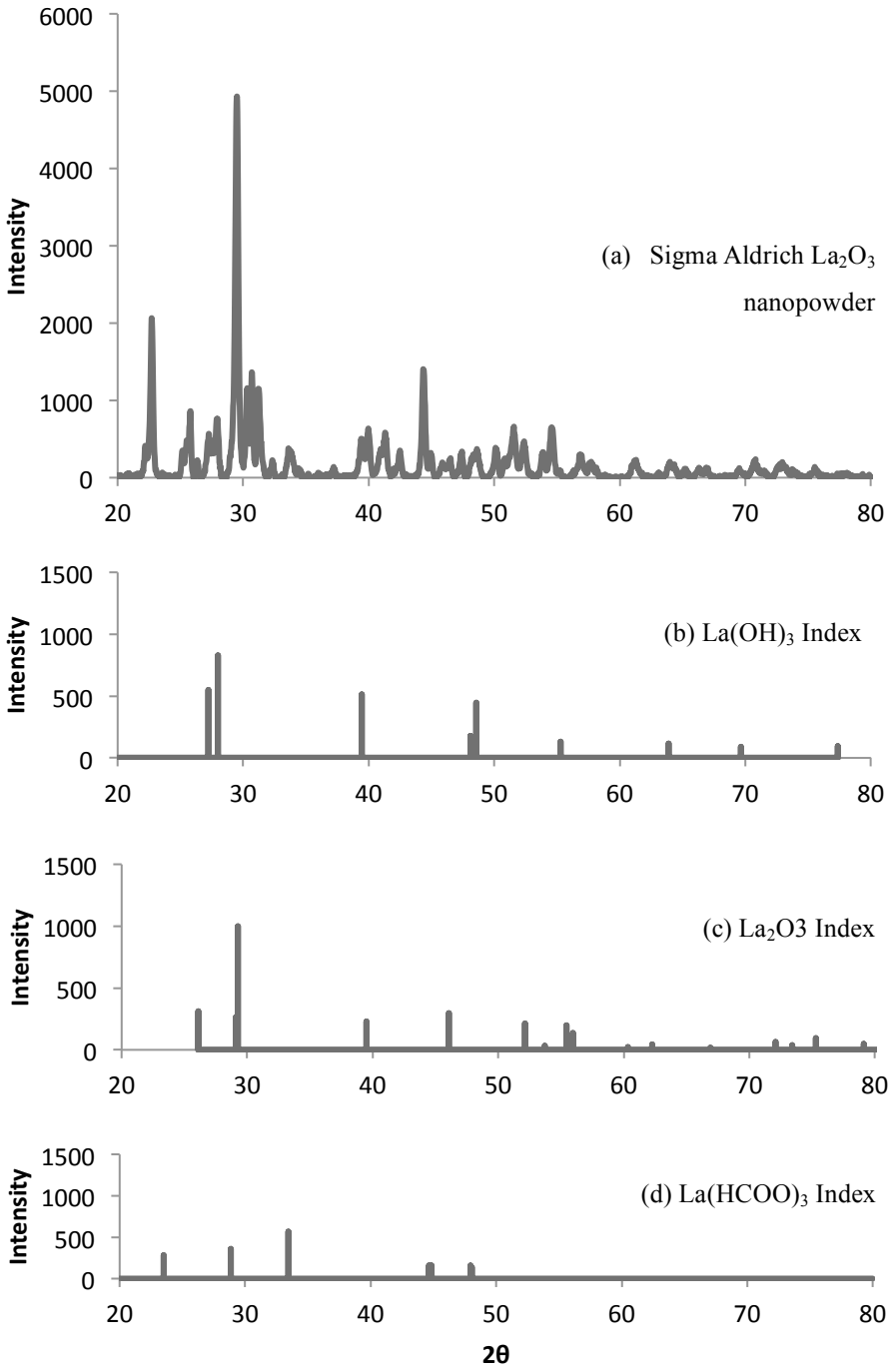

Figure 4-3. XRD patterns for purchased La_2O_3 nanopowder (a) and crystallography indices for (b) $La(OH)_3$ (c) La_2O_3 and (d) $La(HCOO)_3$

4.2 Coating of Commercial La_2O_3 Nanopowder

4.2.1 Initial Coating Study and Characterization

After characterization of the lanthanum nanopowder, initial coating studies were undertaken using a procedure taken from Liao et al. [76]. Amorphous TiO_2 particles were also synthesized following the procedure for coating, but in the absence of the lanthanum nanopowder. Initial measurements of the zeta potential of the lanthanum nanopowder and the amorphous TiO_2 particles in 1mM KCl solution showed the zeta potential of the TiO_2 to be negative at pH > 3 (Figure 4-4) while the lanthanum nanopowder dispersions are positive at pH < 9.2 (Figure 4-4) with a maxima around pH 7.

The coating of SiO_2 particles with titanium has been shown to be optimized at pH values that maximize the attractive potential between the TiO_2 and SiO_2 [94]. However, pH also influences the solubility of the lanthanum particles. Initial laboratory experiments revealed significant dissolution of lanthanum powder at pH < 6 (see Appendix), supporting the work of Chanaud et al. [95] that showed La^{3+} cations do not undergo significant hydrolysis and condensation until pH > 6. To observe the effects of initial pH on the coating, HCl and NH_4OH were added to the initial lanthanum nanopowder dispersion to adjust the pH to 5.7 and 12.3, respectively, which compares to 9.8 during the standard procedure. The zeta potential of the amorphous TiO_2 at pH ranging from 3-11 was used as a reference for checking the extent of coating of the lanthanum nanopowder (Figure 4-4). If the nanopowder were completely coated, one would expect the zeta potential curves of the coated material to match that of the amorphous TiO_2. Though the zeta potential curves are shifted slightly more negative, the coating seems to be incomplete. A statistical hypothesis test was performed and determined the coated particles zeta potential was significantly different than the uncoated La_2O_3, and also the amorphous TiO_2 at pH 8.95. Unexpectedly, there is little difference between the standard coating procedure and the coatings performed at different pHs. This was confirmed statistically using an ANOVA test. This can mostly likely be explained by the sharp rise in pH after addition of the titanium precursor solution. Upon addition of the Ti precursor, the solution turns basic, even with the initial pH adjustment. Further control of pH could be done by slowly adding HCl or another acid

via syringe pump in a rate that ensured a constant pH of approximately 6 as the alkoxide was added.

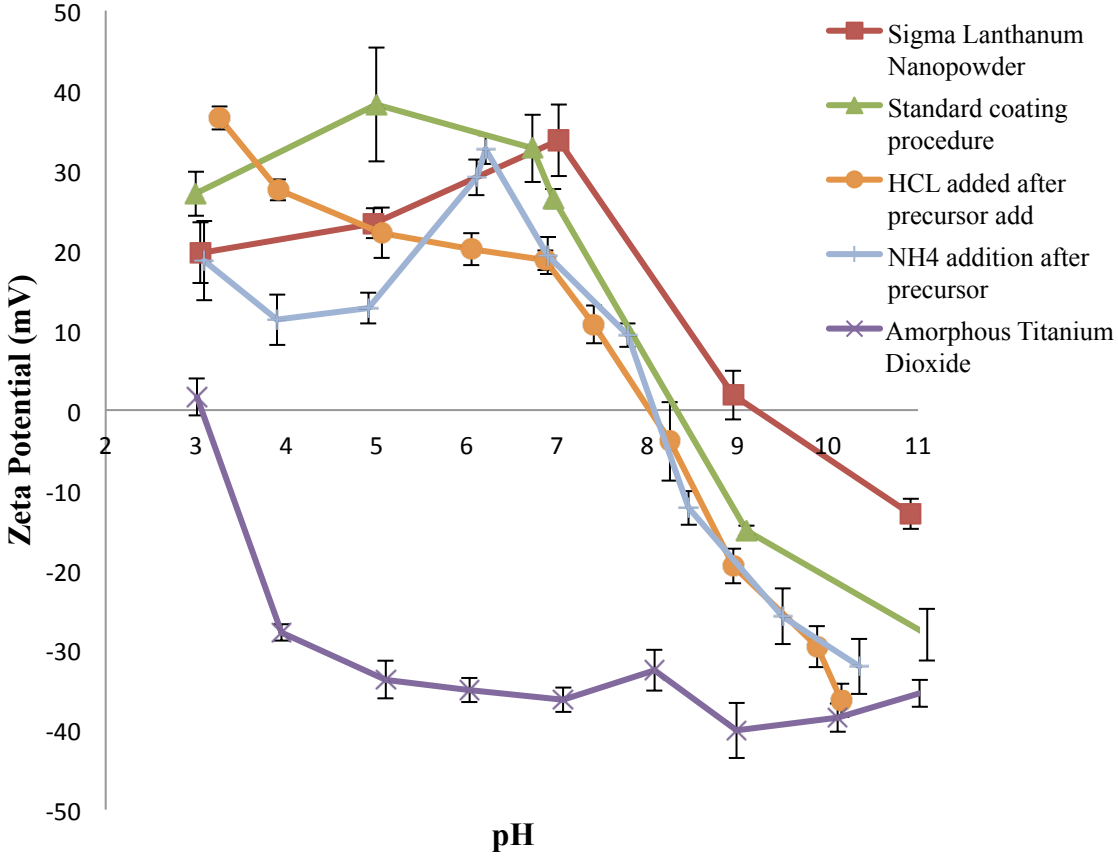

Figure 4-4. Zeta potential of coated commercial lanthanum nanopowder

XRD analysis was performed on the coated and uncoated lanthanum nanopowders, as well as the titanium dioxide particles (Figure 4-5). Titanium dioxide nanoparticles synthesized in the absence of core material reveal no diffraction peaks. This lack of peaks indicates an amorphous material lacking crystalline structure, agreeing with all available literature on coating of materials using titanium alkoxides prior to thermal treatment [70, 76, 80]. As expected, the coated materials show no sign of titania crystal structure prior to heat treatment.

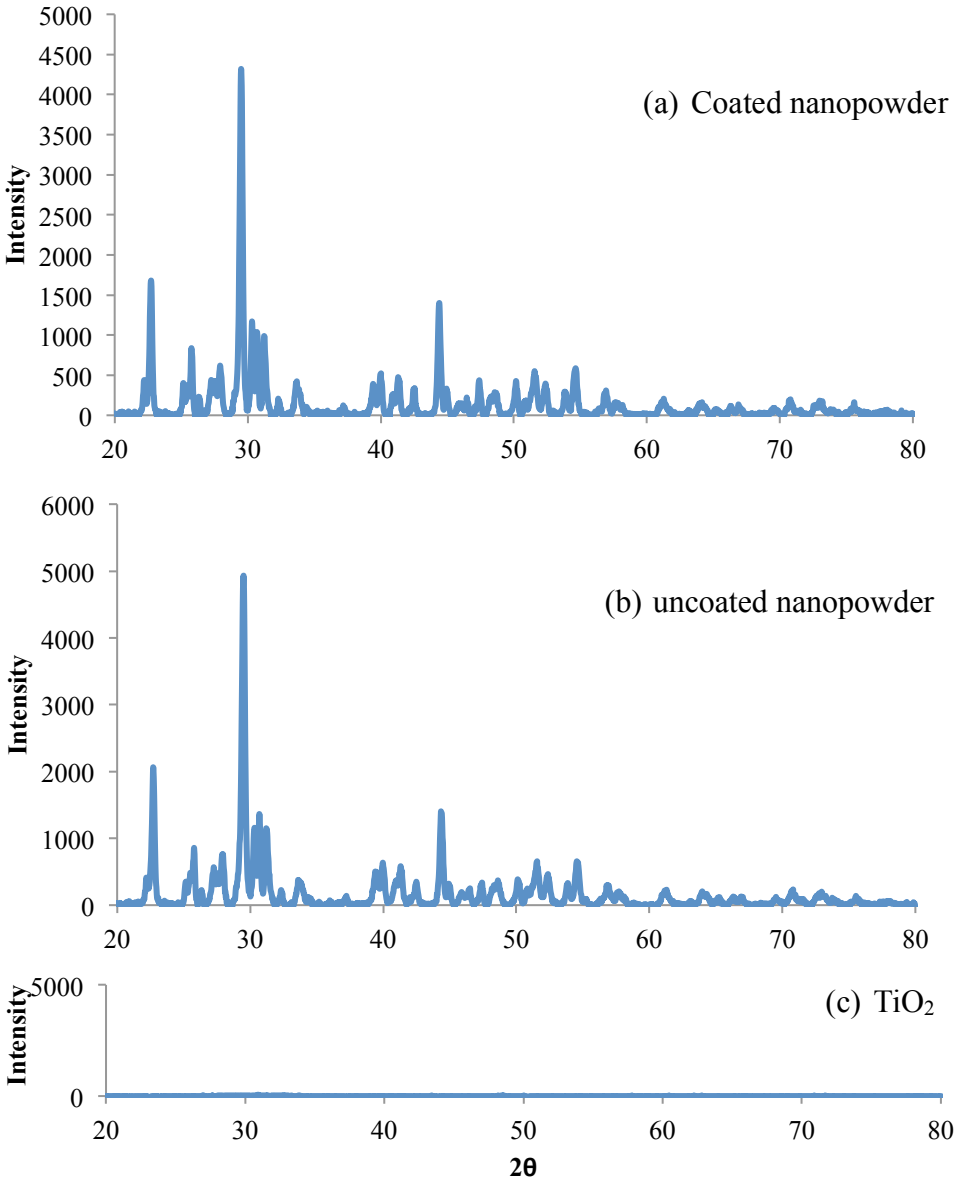

Figure 4-5. XRD patterns for coated nanopowder (a), uncoated nanopowder (b) and amorphous TiO_2 particles (c).

Further study of the morphology of the coated particles was accomplished using several electron microscopy techniques to obtain a more detailed picture of the coating of the lanthanum nanopowder. A typical particle aggregate was chosen for elemental mapping and imaging (Figure 4-6 4-6).

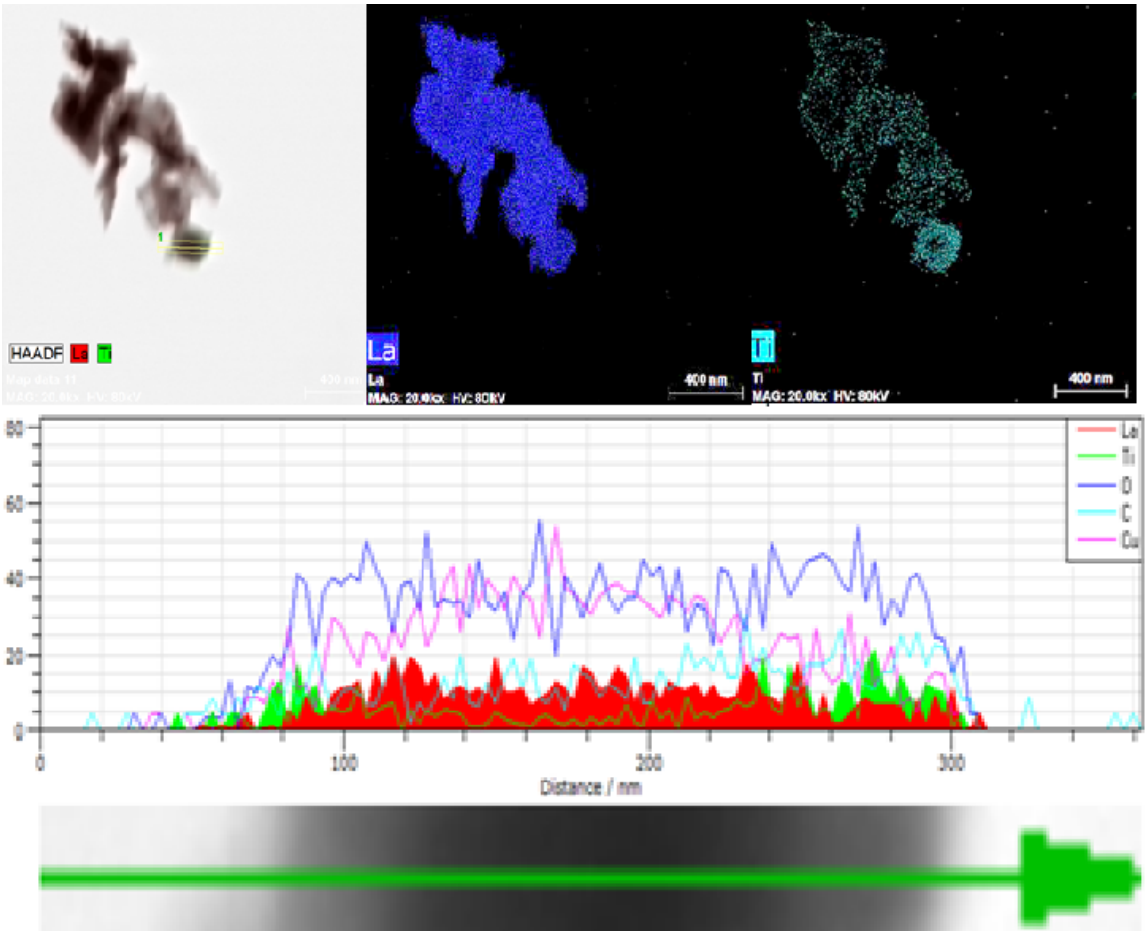

Figure 4-6. HAADF image with accompanying Ti and La maps and EDX line scan (bottom).

It is clear from these images that Ti was deposited on the La particle surface; however, the coating appears thin and non-uniform. The thickness of the titanium coating is an important variable and characteristic, but is one that is not easily discernible in typical TEM mode for these particles. Contrast in TEM imaging comes from differences in atomic numbers, Ti and La being

22 and 57 respectively. However, the thickness of the material can also provide differences in contrast. Due to the polydisperse nature of these core particles, thicknesses vary between aggregates examined, varying contrast in the image and making z contrast differences impossible to discern. To further investigate the coating, a FIB liftout was performed on a large particle aggregate and analyzed in EFTEM mode. The resulting cross section and elemental map can be seen in Figure 4-7. A thin coating of titania appears on the surface of the particle aggregate lending strong evidence of coating of the nanopowder. Although the images indicate coating, the TiO_2 layer is patchy, thin and incomplete which is consistent with the resultant zeta potential curves.

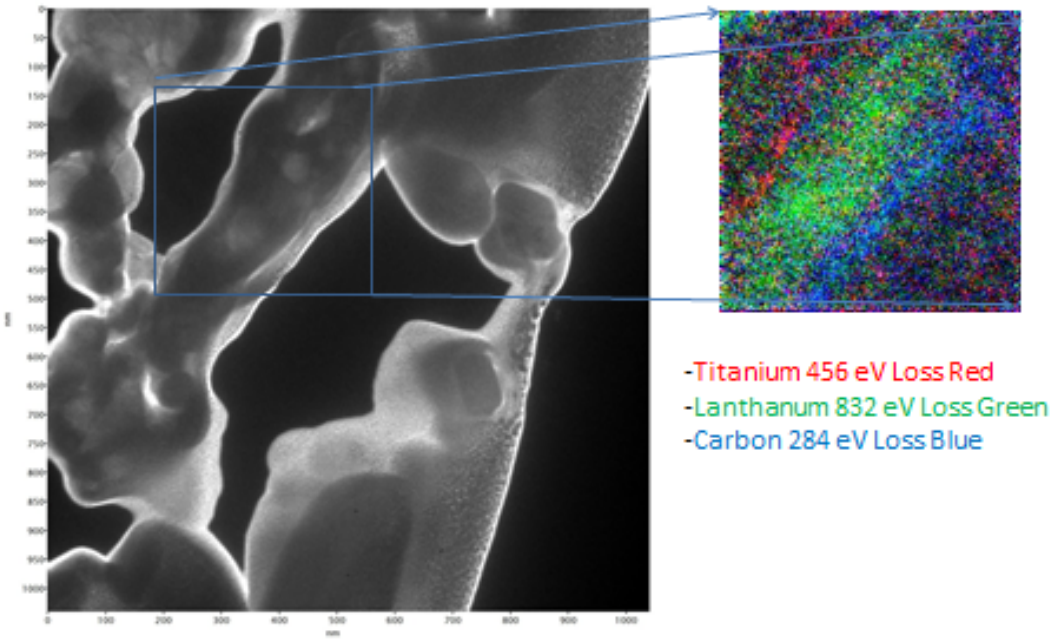

Figure 4-7. EFTEM image of FIB liftout particle aggregates and corresponding EDS map.

4.2.2 Coating study with controlled hydrolysis of TBOT

Initial coating was executed with an excess amount of water, approximately 4.04M. Hsu et al. [70] has shown that TBOT forms precipitates immediately upon mixing when added to solutions containing water concentrations in excess of 0.7M. Initial coating studies detailed in the previous section indicate poor surface coverage of our material. It was hypothesized that by slowing the reaction of TBOT and investigating the effects of water on the coating of the nanopowder, a more complete coverage of TiO_2 could be achieved. Water concentrations of 0.54M and 0.27M H_2O were chosen for investigation. A second variable was added to probe the possibility of creating varying shell thickness by changing the amount of nanopowder added to solution prior to coating. A summary of the experimental parameters and resulting characterization are shown in Table 4-2.

Table 4-2. Sample parameters along with experimental and resulting Properties of La_2O_3/TiO_2

Sample no.	TBOT Conc. (mol/L)	La2O3 NP conc. (g/L)	H2O conc. (mol/L)	Molar Ratio $(Ti:La)_{calc}$	Molar Ratio $(Ti:La)_{exp}$	Zeta Potential (mV) ± std. dev at pH 9.22 ± .17
1	0.015	2.34	0.27	1 : 1	0.020 : 1	-17.46±2.72
2	0.015	2.34	0.54	1 : 1	0.043 : 1	-8.98±1.42
3	0.015	0.97	0.27	2.5 : 1	0.005 : 1	-13.61±2.15
4	0.015	0.97	0.54	2.5 : 1	0.200 : 1	-9.4±2.89
5	0.015	0.49	0.27	5 : 1	0.004 : 1	-21.04±2.19
6	0.015	0.49	0.54	5 : 1	0.167 : 1	-11.91±14.35
7	0.015	0	0.54	n/a	n/a	-40.08±3.47

The lanthanum nanoparticles can essentially be thought of seeds for titanium growth. For any given water concentration and TBOT concentration, a certain amount of solid TiO_2 should be produced. If fewer core particles are present, the coating of the lanthanum nanopowder should

be thicker than those samples with larger amounts of particles. Unfortunately, with the polydisperse nature of the starting material, an increase in diameter could not be quantified via DLS.

As seen in Table 4-2, experimental values of Ti:La are very small compared to the calculated values assuming complete hydrolysis. For both the 0.54M and 0.27M H_2O samples, water is in excess and should yield full formation of titanium solids from the precursor solution. The lack of complete hydrolysis indicates the rate is quite slow for this system or not enough water is present to complete the reaction. It is possible that during rinsing/washing titanium precipitates formed could have been lost during the decanting of the supernatant Mass balances were not performed on this coating procedure but would have helped account for the remaining unreacted titanium precursor. For all cases, the amount of titanium hydrolyzed into particle form is lower for samples synthesized in 0.27M H_2O conditions. Differences in Ti:La ratios between 0.27M and 0.54M water concentrations indicate it is an important variable in the coating of the material. Ocana et al. found that 0.54M ratios created significantly thicker coatings.

Figure 4-8 displays the zeta potential titrations performed on the particles coated with water concentrations of 0.54 M. The zeta potential curves for the 3 coated samples closely resemble each other, even though the Ti:La ratios vary greatly between the 3 samples. A hypothesis test reveals there is no significant different on zeta potential values at pH 9.22. Results for the samples coated at 0.27M H_2O follow the same trend as those with 0.54M H_2O and can be found in the Appendix. Samples 4 and 6 have Ti:La ratios of 0.2:1 and 0.167:1, respectively, much higher than that of sample 2; however, the IEPs are roughly the same. It is hypothesized the similarities in the zeta potential curves, despite vastly different Ti:La ratios, is due to similar degrees of surface coverage with varying thicknesses between samples. As seen in the initial coating experiment, coating seems to be incomplete. Changing the ratio of Ti:La in the system does not appear to change the electrostatic properties of the coated particles, indicating something other than the hydrolysis rate of the precursor as a key factor in the coating of the lanthanum nanopowder. A possible explanation of the seemingly preferential coating is the polycrystalline structure of the core material. The crystallinity of the lanthanum powder, as seen earlier, is not well defined and consists of many different crystalline phases. Though the coating

is amorphous, a likely cause of the preferential coating is differences in crystal structure on the surface of the lanthanum nanopowder. Lattice mismatching has shown to make the creation of core-shell materials much more difficult [96].

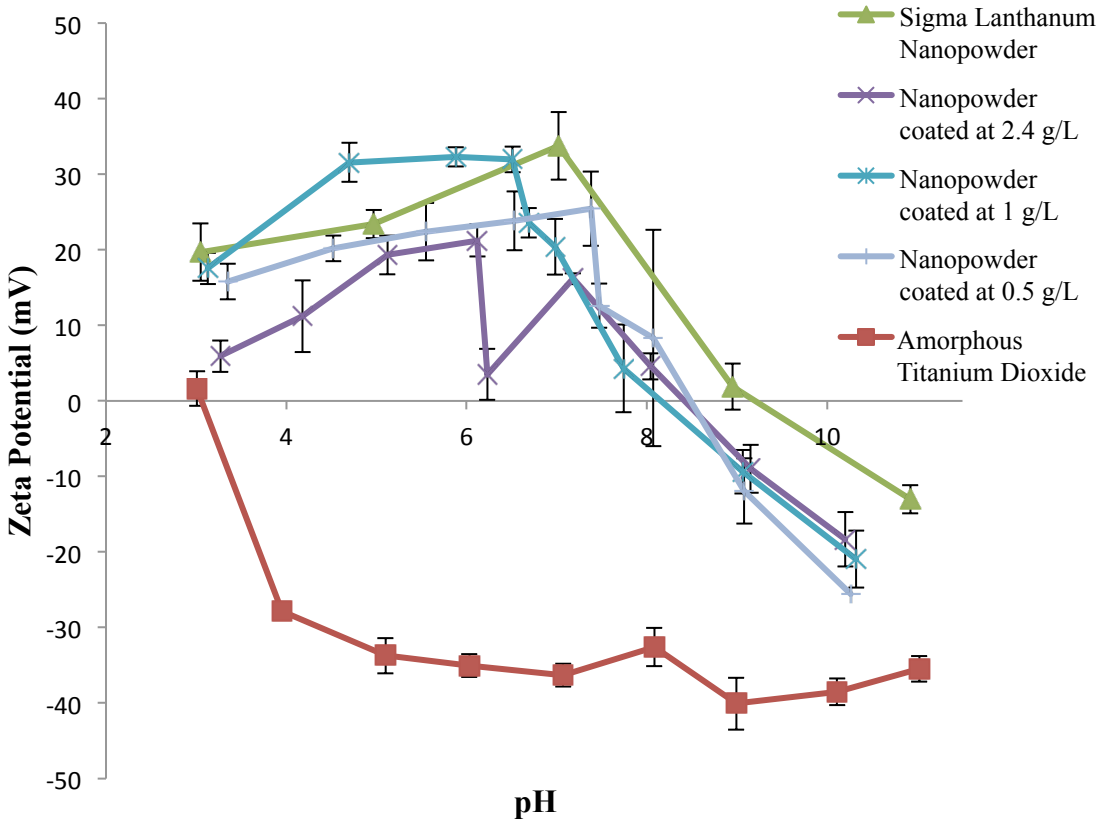

Figure 4-8. Zeta Potential curves of coated Lanthanum nanopowder at 0.54M H_2O

The seemingly preferential coating of the lanthanum nanopowder is hypothesized to be due to the decrease in the Gibbs free energy needed for heterogeneous nucleation of the titanium precursors on different crystal facets of the lanthanum particle surface. Heterogenous nucleation can be expressed in the following equation [97]:

$$\Delta G_{interf} = \bar{\gamma}_{CW} A_{CW} + (\bar{\gamma}_{CS} - \bar{\gamma}_{SW}) A_{CS}$$

Where the suffixes CW, CS, and SW refer to cluster-water, cluster-substrate, and substrate-water respectively. When the solid substrate, the lanthanum particle surface, is a good match for the

crystals being formed, TiO_2, the cluster-water interfacial energy becomes much greater the than the cluster-surface interfacial energy and the Gibbs free energy for formation becomes

$$\Delta G_{interf} = \bar{\gamma}_{CW} A_{CW}$$

In this case, the heterogeneous nucleation on the surface of the core particles becomes much easier. It is evident in the zeta potential curves that poor surface coverage of the material occurred. Examination of the XRD patterns in Figure 4-3 indicate the oxide phase as dominant, leading to the conclusion that either the carbonate or hydroxide phase is a better match for coating. To examine this hypothesis, $La(OH)_3$ particles were synthesized and coated as described in the following sections.

4.3 Characterization of synthesized $La(OH)_3$

In order to have a more monodisperse core-material with well-defined crystallinity, $La(OH)_3$ nanospheres were synthesized under hydrothermal conditions using a modification of the procedure described by Tang et al. [18]. In the original procedure, telfon lined steel autoclaves were filled to 80% of their capacity before treating at 180°C for 12 hours. Experiments were carried out at 66% of the total volume of the steel autoclave due to safety precautions, resulting in smaller crystallite sizes. Particle sizes measured by DLS, TEM, XRD, and SAXS are shown in Table 4-3.

Table 4-3. $La(OH)_3$ particle size measurements by DLS, TEM, XRD, and SAXS

Method	Size (nm)
DLS	50.4-259.5
TEM	8.54±1.95
Scherrer Analysis of XRD patterns	9.32
SAXS	15

Particle sizes measured by TEM and XRD agree very well, which is expected as both quantify the primary particle size even if contained in a larger aggregate. SAXS analysis yielded slightly larger particle sizes. Measurements for SAXS analysis were done at 3 concentrations

and the corresponding curves can be found in the Appendix. Single size distributions were found for samples at 100 ppm and 10 ppm , however a bimodal distribution occurred when size was analyzed at 1 ppm. This bimodal distribution suggests there could be aggregation of primary particles. DLS results also indicate particle aggregation with all measurements resulting in sizes greater than 50.4 nm. The nature of DLS is such that scattering intensities are proportional to diameter raised to the 6^{th} power [85]; thus, any aggregates in solution will greatly skew the reported hydrodynamic diameter to larger sizes. This particle aggregation can also be seen on the resulting TEM image shown in Figure 4-9. The particles appear to be roughly spherical and highly aggregated, though aggregation could easily occur during the samples preparation.

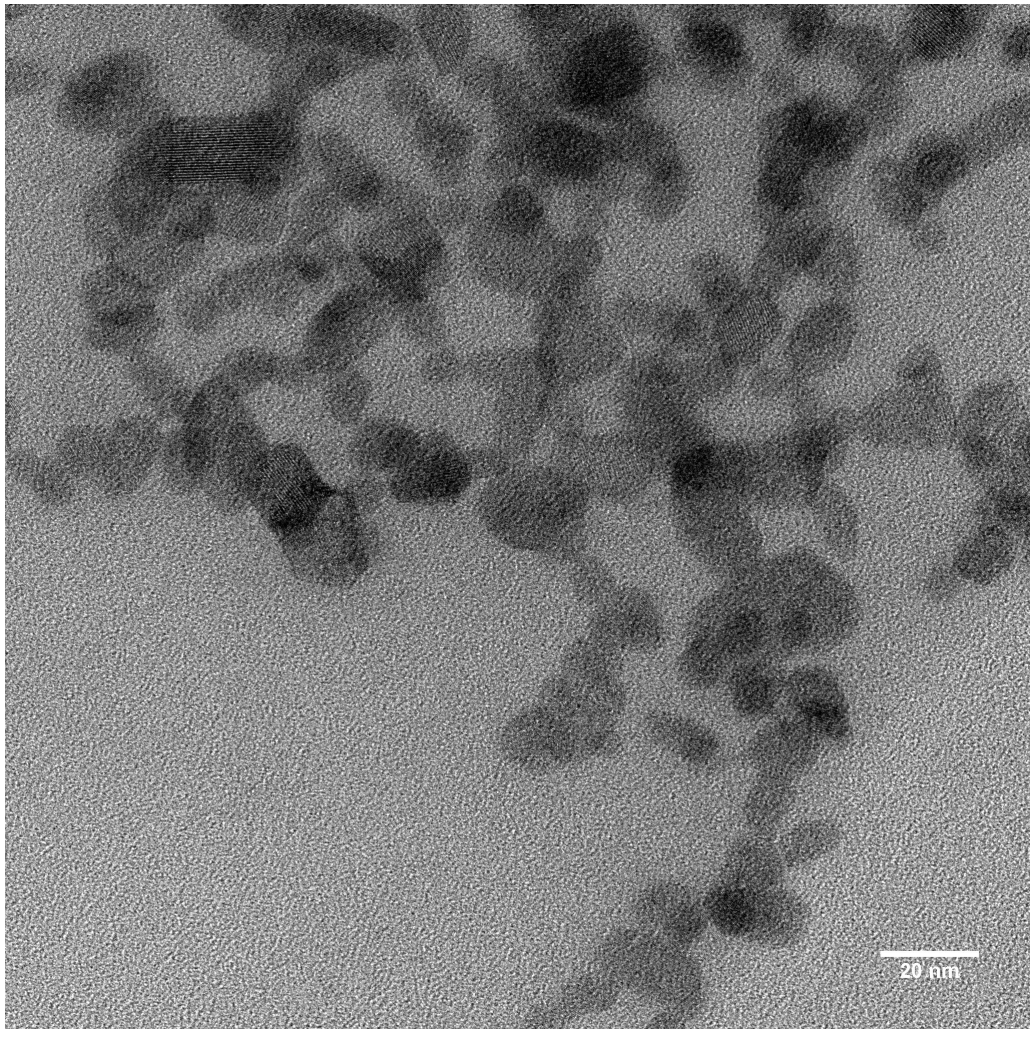

Figure 4-9. TEM image of synthesized $La(OH)_3$

Primary particles of $La(OH)_3$ undergo aggregation either during synthesis or during the washing/rinsing procedure. Aggregation was investigated by altering the washing/rinsing procedure and through the addition of surfactants Triton X100 and CTAB. Citrate is commonly used as a stabilizing agent in the synthesis of nanomaterials such as gold. Analysis of the washed $La(OH)_3$ particles using FTIR indicated that washing and rinsing of the $La(OH)_3$ completely removed citrate from the particle surface (see Appendix). In an attempt to reduce aggregation, particles were washed and rinsed in a citrate containing DDI solution and a DDI solution adjusted to pH 11, and the size of the resulting particles were measured by DLS. The size of the particles rinsed in a pH adjusted solution was 81.1±2.8 nm and the diameter of the citrate washed particles was between 500-600 nm. These results suggest that the adjustment of the pH had a positive effect on the stabilization of the material while the citrate addition did not. It is possible that washing in a pH adjusted citrate rinse would have been more successful; however, that was not investigated.

To further examine the aggregation behavior, zeta potential titrations were performed on the particles washed in citrate and particles with the citrate removed (Figure 4-10). The zeta potential for the citrate-free particles appears quite standard and is in agreement with reported values on the IEP of $La(OH)_3$ [98]. The zeta potential curve of the citrate-washed particles, however, is quite different. Particles are negatively charged over the entire pH range, becoming more negative away from approximately pH 6. Hydrodynamic diameters of citrate-free particles were measured at varying pHs and are also shown in Figure 4-10. Particles are stable around 71 nm for pH > 6.5, but aggregation occurs as pH is decreased further. One would expect this aggregation of particles to occur around the IEP of 8.3. Further investigation is needed to explain this phenomenon. The effects of rinsing the particles after synthesis with pH adjusted solution agree the results found in Figure 4-9.

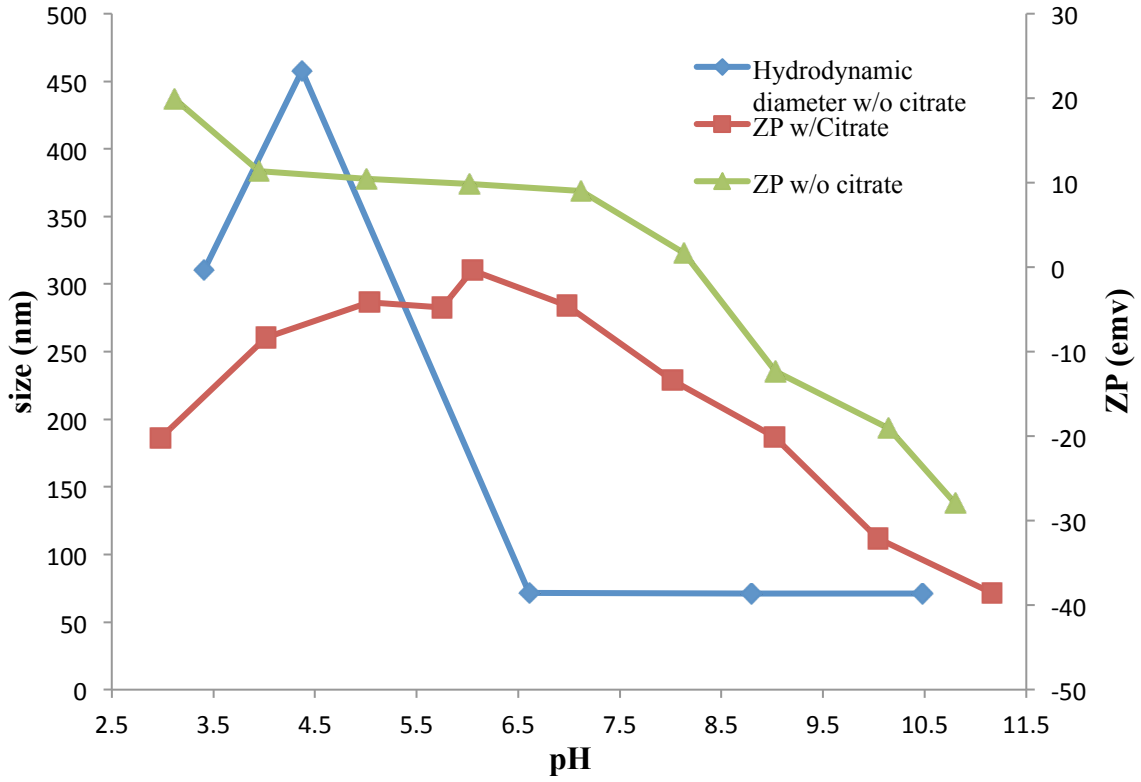

Figure 4-10. Zeta potential and hydrodynamic diameters of $La(OH)_3$ at various pH values

Although aggregation does seem to occur if particles are not washed and rinsed in pH adjusted solutions, particle aggregation is clearly still occurring during the hydrothermal synthesis despite the fact that the pH is approximately 13.35 and zeta potential analysis indicates electrostatic stability at that pH. In efforts to limit this aggregation, two surfactants, CTAB and Triton X100, were evaluated for their ability to inhibit aggregation of the $La(OH)_3$ nanoparticles. CTAB is a cationic surfactant commonly used in the synthesis of nanomaterials such as $La(OH)_3$ nanorods [83]. Triton X100 is a nonionic surfactant that has shown to stabilize nanomaterials [99]. In separate trials, each surfactant was added either before synthesis or after synthesis to see if stable particle suspensions of individual primary particles could be obtained. The resultant

hydrodynamic diameters are shown in Table 4-4. Hydrodynamic diameters of particles synthesized with CTAB are similar to particles synthesized without any surfactant while the Triton X100 seemed to enhance aggregation. Average diameters of Triton X100 synthesized and CTAB synthesized particles are 577.93±250.35 and 190.1±83.09 respectively. Though there is a wide variation in particle size measurements, especially for the Triton X100 synthesized particles, hypothesis testing of the particle sizes yielded a significant difference in size. CTAB is thought to provide a better stabilization of the material because of its cationic properties. At basic pH, $La(OH)_3$ particles are negatively charged, resulting in an attraction between the positively charged surfactant and the negatively charged particles. However, CTAB has been known to bind to certain crystal facets, possibly inhibiting growth in that direction and encouraging the formation of nanorods [83]. The formation of nanorods during synthesis with CTAB could explain larger hydrodynamic diameters measured by DLS. However, further investigation by TEM would need to be carried out to confirm this hypothesis.

Table 4-4. Hydrodynamic diameters of particles synthesized with surfactants

Sample	D_H (nm) by DLS
$La(OH)_3$ synthesized w/Triton X100	288.9-727.2
$La(OH)_3$ synthesized w/CTAB	113-278.1

The crystal phase of the synthesized particles was determined by XRD (Figure 4-11) and can be indexed primarily to hexagonal $La(OH)_3$, while small evidence of other phases are evident. The stability of this phase when exposed to water makes it much more suitable for coating of the material with titanium dioxide as water is an important reagent in the reaction of titanium alkoxides to form TiO_2. If surface sites of La_2O_3 undergo transformation into the hydroxide phase, this reaction will most likely compete with the reaction of titanium precursors on the surface of the core material. The high number of hydroxides bound to the surface of the particle in this phase also allows for the possibility of generating a very thin coating of titanium without the presence of water at all, eliminating the potential for the homogeneous nucleation of TiO_2 nanoparticles during coating.

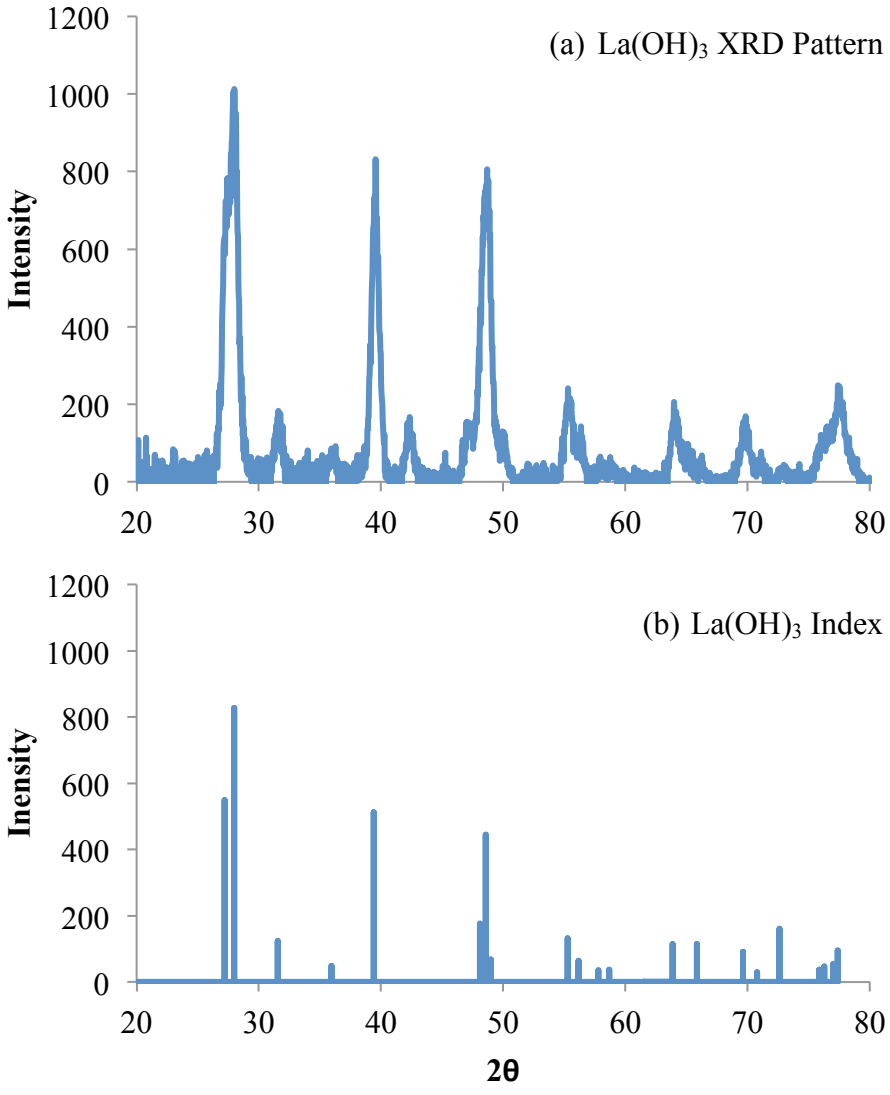

Figure 4-11. XRD pattern of synthesized $La(OH)_3$ (a) and corresponding index values for $La(OH)_3$ (b)

4.4 Coating of $La(OH)_3$ Nanoparticles

$La(OH)_3$ nanospheres were coated in both 0.54M water and in the absence of water. Zeta potential titrations were performed as an initial indication of coating efficacy (Figure 4-12). Zeta potential curves for the coated lanthanum hydroxide material closely match that of the amorphous titania particles created in the absence of the core material. Statistical analysis of the zeta potentials at pH 5.95 indicates no significant difference in measurements, yielding a good match. The similarities between the zeta potential of material synthesized with and without water indicate sufficient hydroxyl groups present on the surface of the coated material to hydrolyze the TBOT precursor. Zeta potential curves for the two coated materials seem to indicate a good titanium coverage of the $La(OH)_3$ nanospheres.

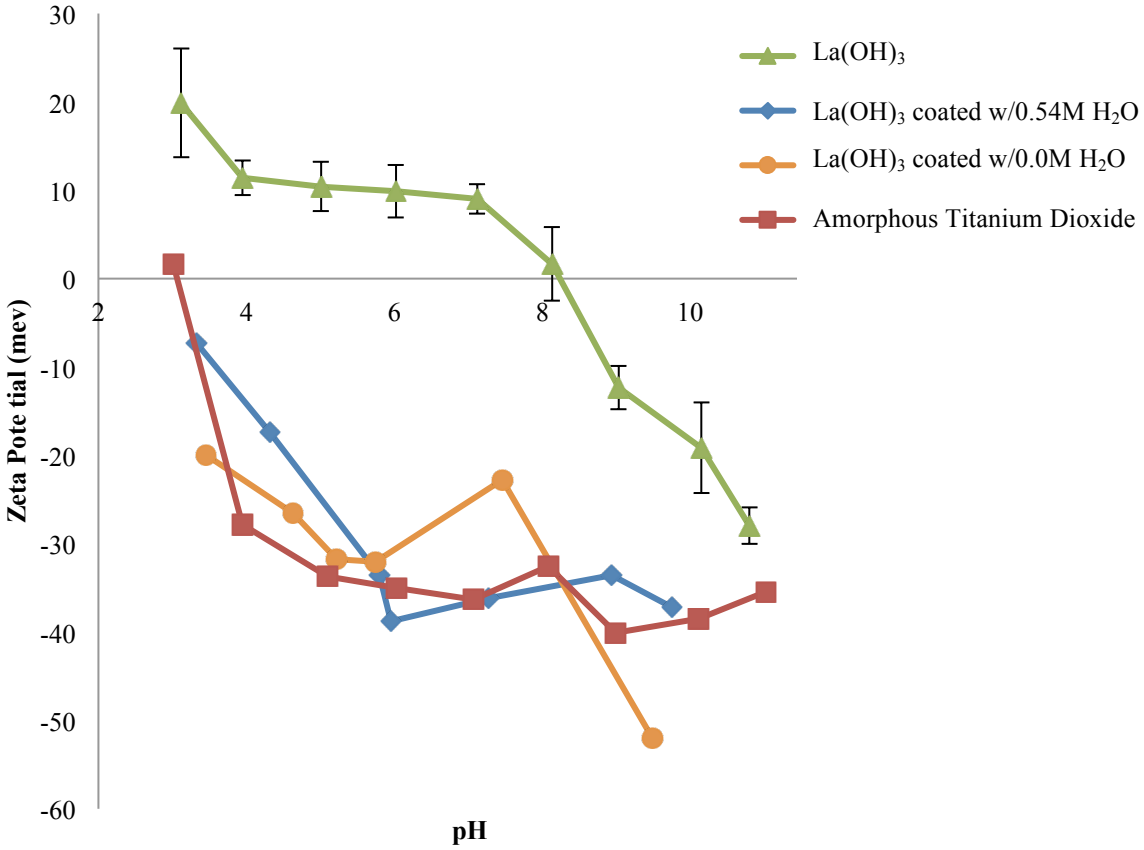

Figure 4-12. Zeta potential curves for coated $La(OH)_3$ nanospheres

Further study of the coated materials was performed using TEM imaging. With coated materials, TEM imaging should allow for the validation of a core-shell structure; however, such evidence was not found (Figure 4-13). As reported earlier, contrast in TEM imaging results from differences in atomic number. The difference in atomic numbers between La and Ti should clearly be seen on TEM images. Because contrast also arises from differences in sample thickness, a possible explanation of this lack of visual core-shell structure is that the resultant titanium coatings are very thin. Resolution of incredibly thin coatings would be difficult to resolve via TEM. Figure 4-13 does reveal less individual particle structure than images of uncoated lanthanum hydroxide seen in Figure 4-9. A thin coating of amorphous material over an aggregate of particles could explain this phenomenon. The examination of core-shell morphology is made much more difficult when particles are heavily aggregated. Examination of individual particle coatings was simply not possible.

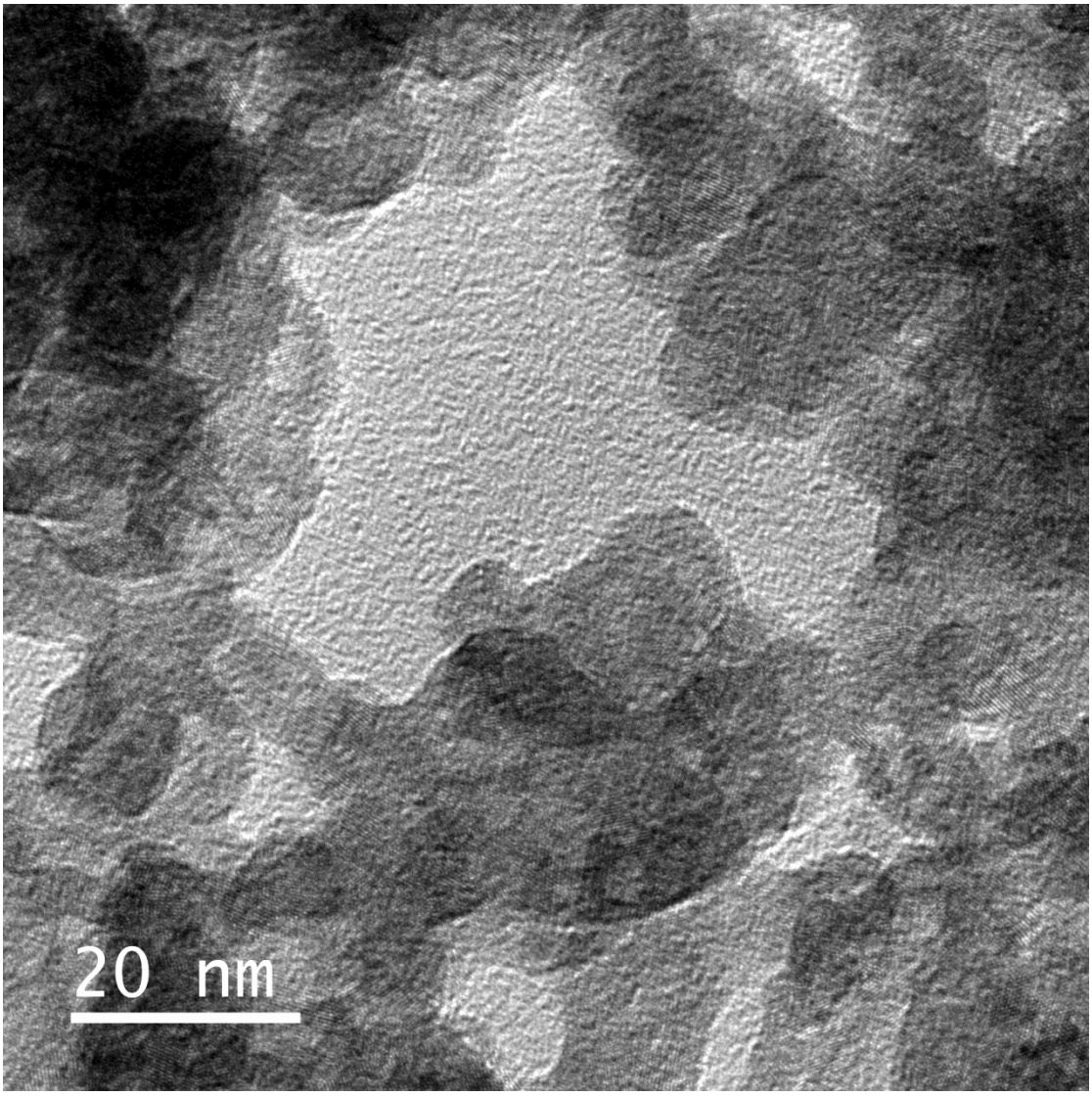

Figure 4-13. TEM image of coated $La(OH)_3$ at 0.54M water concentration

EDS maps of $La(OH)_3$ aggregates coated in the presence and absence of water were created to confirm the presence of a TiO_2 coating. The resultant maps can be found below in Figures 4-14 and 4-15 for the two synthesis conditions. The maps of the material coated with water show strong evidence of titanium coating, while the maps from the sample synthesized without water indicate very little to no titanium. However, coatings consisting of only several molecules of titanium are well beyond the detection limits of EDX. Ti:La ratios found in the

maps for the water synthesized coatings are approximately 1:249 by weight and 1: 86 by atomic percent. Tables of these values can be found in the Appendix. This small ratio suggests coating occurred, but was very thin. Ratios are very similar to the Ti:La ratios found for the coated La_2O_3 nanopowder discussed earlier. Analysis of the titanium maps for the particles coated without water yielded 0% Ti by weight.

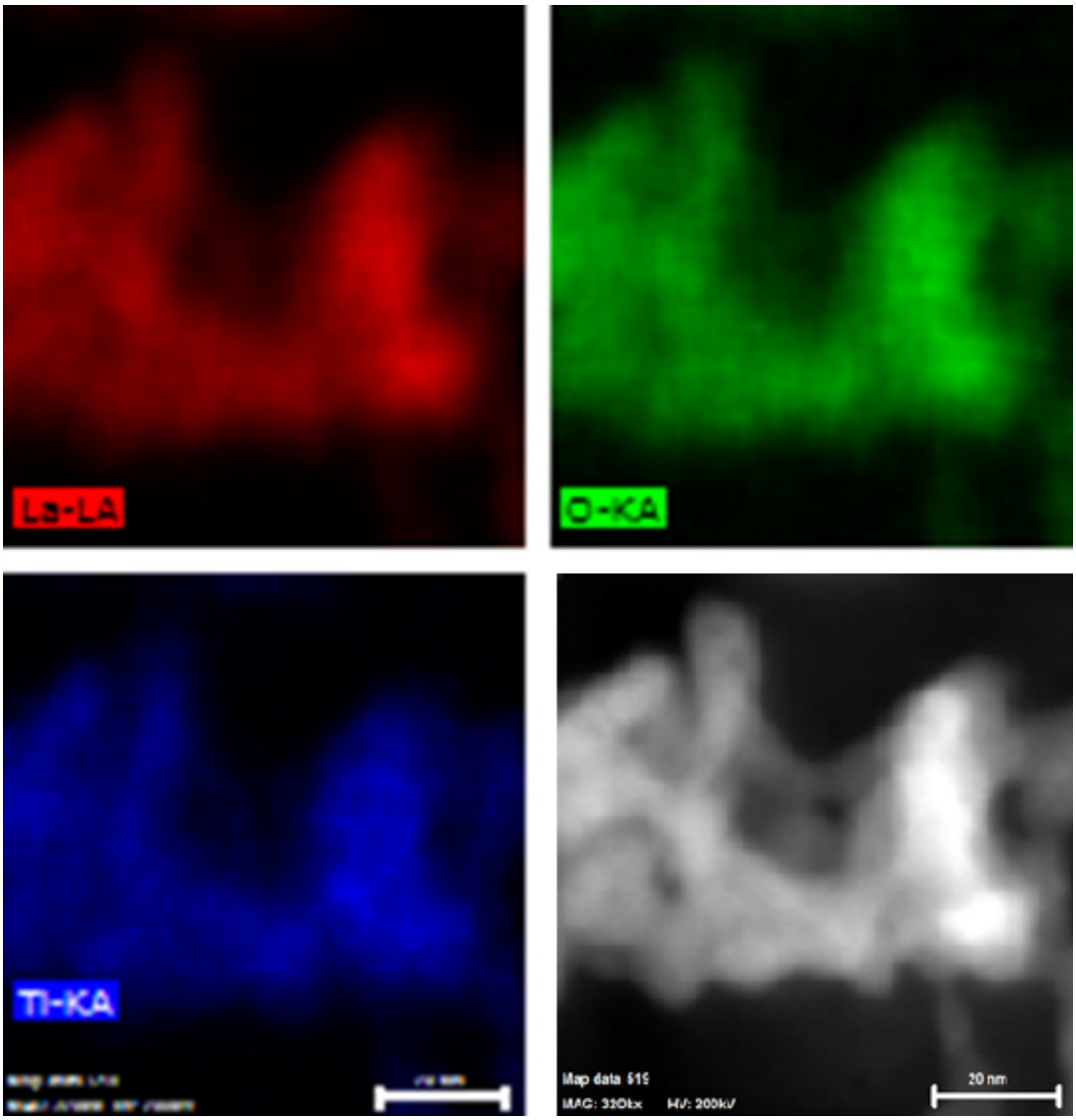

Figure 4-14. Elemental maps of coated $La(OH)_3$ synthesized at 0.54M water concentrations

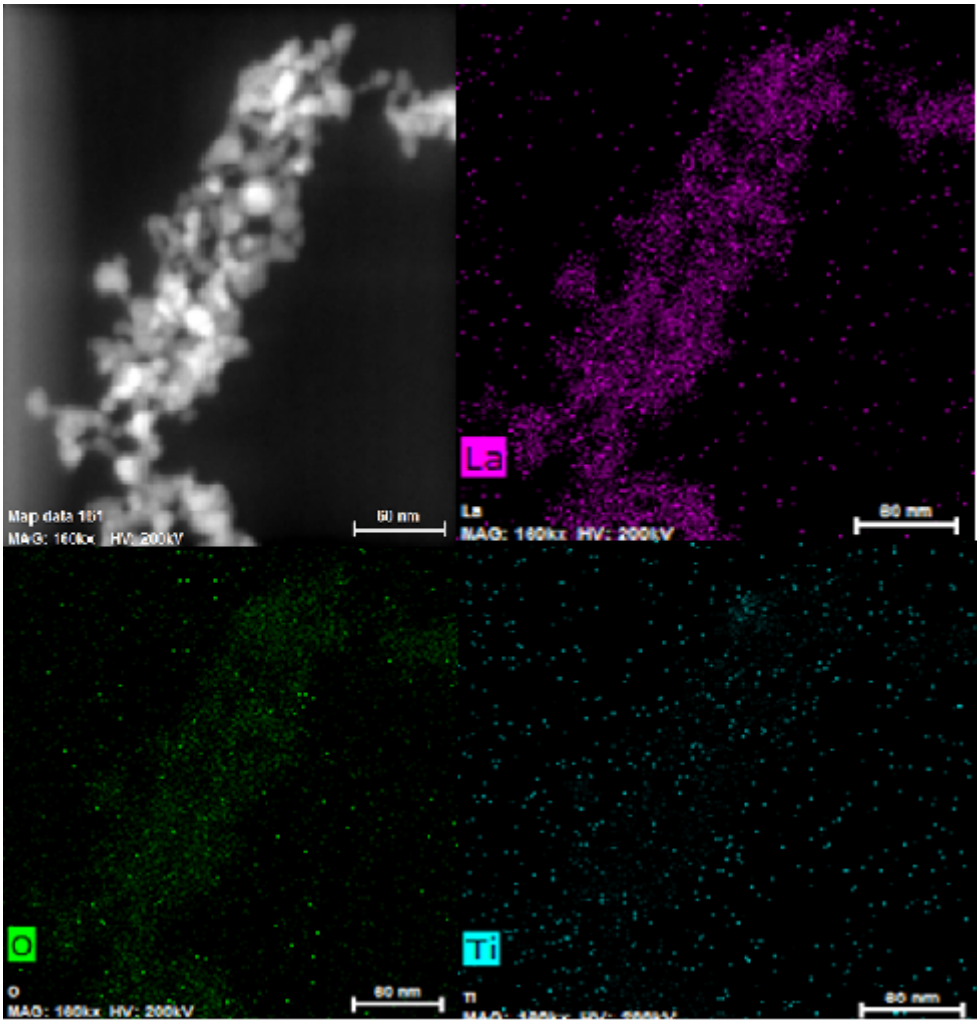

Figure 4-15. Elemental Maps of $La(OH)_3$ particles coated in the absence of water

4.4.1 Examination of the effects of temperature and Ti precursor on particle coating

The data presented thus far does not show evidence of the generation of titanium precipitates in the coating of lanthanum core material. It is, however, evident from the comparison of calculated to experimental Ti:La ratios that incomplete hydrolysis occurred. To ensure this was the case, mass balances were performed on the final coating procedure to ensure

the molar ratios of TBOT added were indeed correct. In an attempt to increase the rate of hydrolysis and thereby increase the thickness of the titanium shell, coating procedures were repeated with 0.54M water and zero water, but in sealed glass test vials at 100°C. The primary coating procedure was done at room temperature. Samples were also coated with heat in sealed vials but using titanium tetraisopropoxide (TTIP) as a precursor. TTIP has a shorter alkoxy group then TBOT, making it more reactive [69]. The zeta potential of each suspension of coated $La(OH)_3$ was measured at pH 3.9, at which the zeta potential of $La(OH)_3$ is approximately +10 mV, and compared to amorphous titanium samples as evidence of coating. Zeta potentials for all 4 samples were analyzed statistically and found to be not significantly different than that of amorphous titanium, indicating successful coating of the $La(OH)_3$. However the resultant Ti:La ratios are drastically different for the samples coated using TTIP as a precursor. Coating of the material in TTIP seems to provide a much more robust coating then the slower TBOT.

Table 4-5. Zeta Potentials and molar ratios of samples coated at 90°C with TBOT and TTIP

Sample no.	**Precursor**	**[H_2O] (M)**	**Ti:La (weight)**	**Zeta Potential at pH 3.9 (mV) ± std. dev.**
1	TBOT	0	0.40486	-3.53±1.16
2	TBOT	0.54	0.08542	-2.41±1.83
3	TTIP	0	0.13472	-0.57±3.02
4	TTIP	0.54	0.30303	-3.23±1.42
Amorphous TiO_2	TBOT	0.54	n/a	-1.94±2.29

TEM imaging and elemental maps of the TTIP coated particles can be found in the Appendix. A dedicated line scan across a particle aggregate was performed and the results are shown in Figure 4-16. Resulting mass ratios in the middle of the particle agglomerate as measured by examining EDS maps closely match those quantified by ICP-AES measurements (Table 4-5). More interesting is the longitudinal profile of the line scan. Titanium is present in larger ratios at the edge of the particle, where one would expect to see only titanium if particles were successfully coated. This linescan data suggests strongly that $La(OH)_3$ was coated by an

amorphous layer of TiO_2 approximately around 2 nm in thickness (see raw data counts in the Appendix).

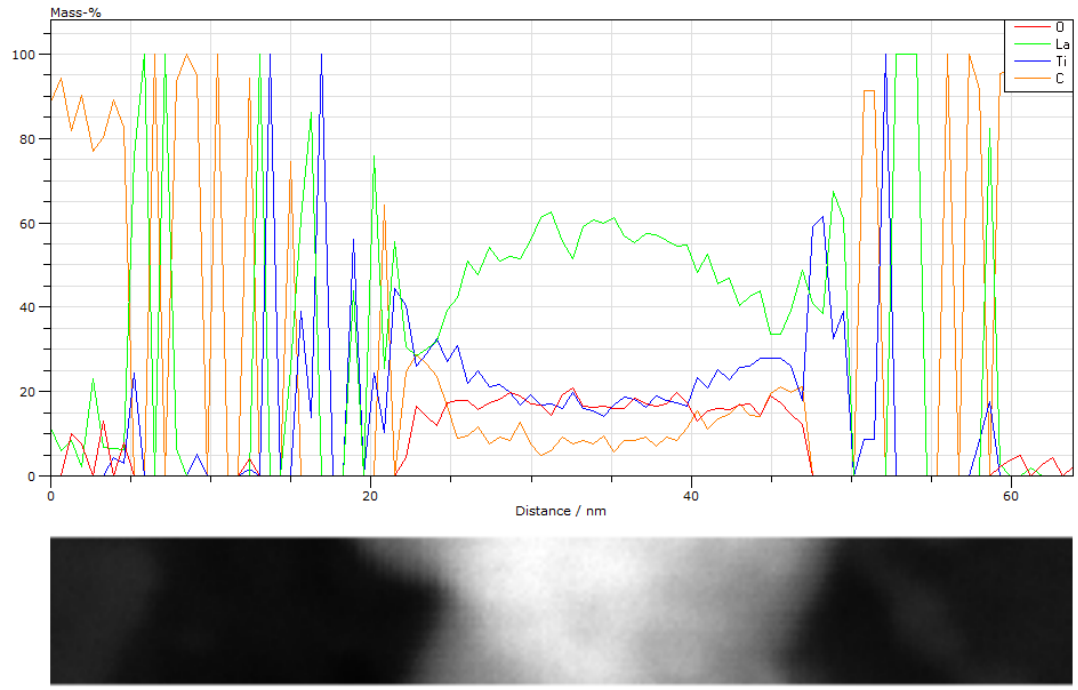

Figure 4-16. EDX Line scan data of $La(OH)_3$ particles coated using TTIP

SAXS analysis was performed on the particles coated with TTIP and TBOT in 0.54M water. The data for the TTIP coated sample is presented in Figure 4-17. The results were compared to data for the $La(OH)_3$ nanospheres used for coating. Fitting of the TTIP data required a 3 population model. Population 1 consisted of an average diameter of 17 nm, whereas populations 2 and 3 had average diameters of 0.9 nm and 0.21 nm, respectively. These multiple populations suggest TTIP coated the $La(OH)_3$ nanospheres in a roughly 1 nm thick coating, and also formed precipitates of titanium, though no evidence of this was visible on TEM imaging. The disagreement between TEM and SAXS data on the formation of TiO_2 precipitates highlights the need for complementary analysis techniques. A complete picture of these nano-systems is obtained more thoroughly by using several analytical techniques.

Assuming a 1 nm shell thickness, and using ρ_{TiO2} = 3.59 to 3.73 g/cm^3 [100] and $\rho_{La(OH)3}$ = 4.29 g/cm^3 one can calculate the theoretical volumes of the core and shell material and

compare those to the actual volumes of materials estimated from metals concentrations measured by ICP-AES. The ratio of theoretical volume to actual volume of shell material is approximately 1.02 to 0.94 based on the density range reported The fact that this value is very close to 1, along with the agreement of La:Ti ratios between TEM and ICP-AES measurements, suggests that the volume of the titanium precipitates generated is very small. SAXS was also used to analyze sample 2. The diameter from these coated particles was measured as being smaller than the original core $La(OH)_3$ particles. This is thought to be due to variations in measurement. As such, conclusions cannot be made regarding the coating thickness. The SAXS curves for the TBOT sample are included in the Appendix. No secondary populations (heteronucleates) were present in the TBOT coated sample. The lack of substantial increase in diameter with the TBOT samples indicates heating did not have a significant impact on the coating of $La(OH)_3$. Further analysis of the effects of temperature should be done by comparing SAXS curves for TTIP coated samples without the addition of heat to the data presented in Figure 4-17.

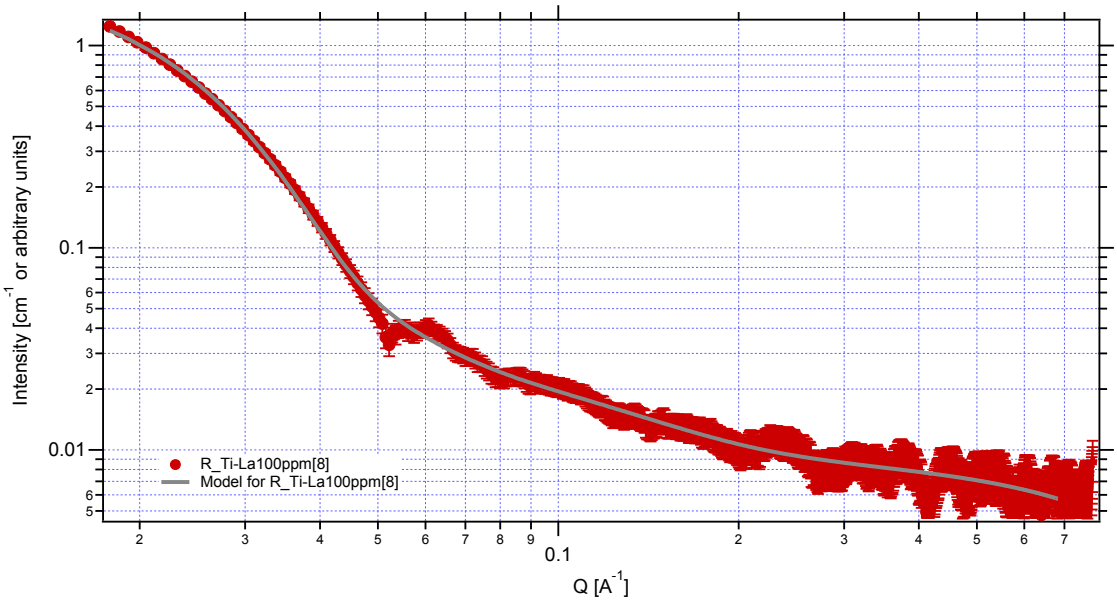

Figure 4-17. SAXS analysis of TTIP coated $La(OH)_3$

4.5 Nitric Acid Stability Test

Although evidence strongly suggests successful coating of $La(OH)_3$ by TTIP and TBOT, further investigation of the extent of the coating was performed by probing the stability of dried particles in 5% nitric acid solution. Demirors et al. [80] showed that upon drying, a multitude of different titanium coated particles were stable in nitric acid solutions. It is important to note the coatings in the study by Demirors et al. were much thicker than those presented in this work. They also showed that without drying, severe dissolution occurred because of the porous nature of the titanium shell. The titanium coatings presented in this work are a great deal thinner than particles studied by Demirrors et al.; however, the thin coating should provide some protection against dissolution. The dissolved lanthanum concentrations upon exposure to HNO_3 are found in Table 4-7. Not enough material was recovered by centrifugation and pelletization to test sample 2. Prior to testing the coated particles, initial experiments were done to show dried $La(OH)_3$ rapidly dissolved, and titanium did not. Dissolved metals concentrations were examined immediately upon exposure to acid, and at 1, 5 and 30 minutes after exposure. The results of the initial test can be seen in Table 4-6.

Table 4-6. Initial test of La and Ti particle dissolution

Sample	% immediately dissolved	% dissolved after 1 min	% dissolved after 5 min	% dissolved after 30 min
$La(OH)_3$NPs	94.9	100.2	102.3	101.5
TiO_2 NPs	0.11	0.6	1.05	0.78

Coated particles were exposed to a 5% nitric acid solution and then either immediately filtered or filtered after 5 minutes of exposure. Lanthanum concentrations immediately upon filtering are relatively low, but a complete and consistent coating of $La(OH)_3$ by TiO_2 should provide protection against immediate dissolution by the nitric acid. After 5 minutes, samples 1 and 3 are almost completely dissolved. This suggests the titanium shell created upon coating is porous, and diffusion through the shell after 5 minutes is almost complete. Evidence suggests sample 4 has a much thicker and/or complete coating. The stability test shows only a slight

increase in the dissolved lanthanum after 5 minutes suggesting diffusion through this pore space takes much longer than through that of the thin coatings on samples 1 and 2. The initial dissolved concentration of lanthanum in samples 3 and 4, also suggests that the fast reaction of the TTIP left some of the lanthanum hydroxide uncoated. La is easily dissolvable in acidic pHs. To ensure La was not dissolving in DDI water, coated particles suspended in DDI water were filtered and the filtrate tested by DLS and ICP to ensure no La was dissolved or particles passed through the filter.

Table 4-7. Nitric Acid Stability test for samples found in Table 4-5

Sample	% La dissolved immediately	% La dissolved after 5 minutes
1	2.5	95.6
3	28.9	94.2
4	13.3	17.2

.

4.6 Thermal Transformation of Shell Material

To best serve as a suitable surrogate for commercially available TiO_2, thermal transformation of the amorphous shell to anatase, rutile or a mixture of the two crystal phases is necessary. Amorphous TiO_2 particles and particles of $La(OH)_3$ coated with TTIP at 0.54M water concentrations were hydrothermally treated at 220°C for 12 hours in separate experiments and the resultant XRD patterns are shown in Figure 4-18. The XRD pattern for the hydrothermally treated titanium dioxide can be indexed to the anatase crystal phase, with no evidence of the formation of rutile. Anatase TiO_2 is the only crystalline phase identified in the coated samples, with no evidence of either $La(OH)_3$ or any intermediate Ti-La crystal phases. The typical method for transformations of coated material is high temperature calcination, which can lead to the formation of crystal phases consisting of both core and shell elements in the boundary layer between the core and the shell.

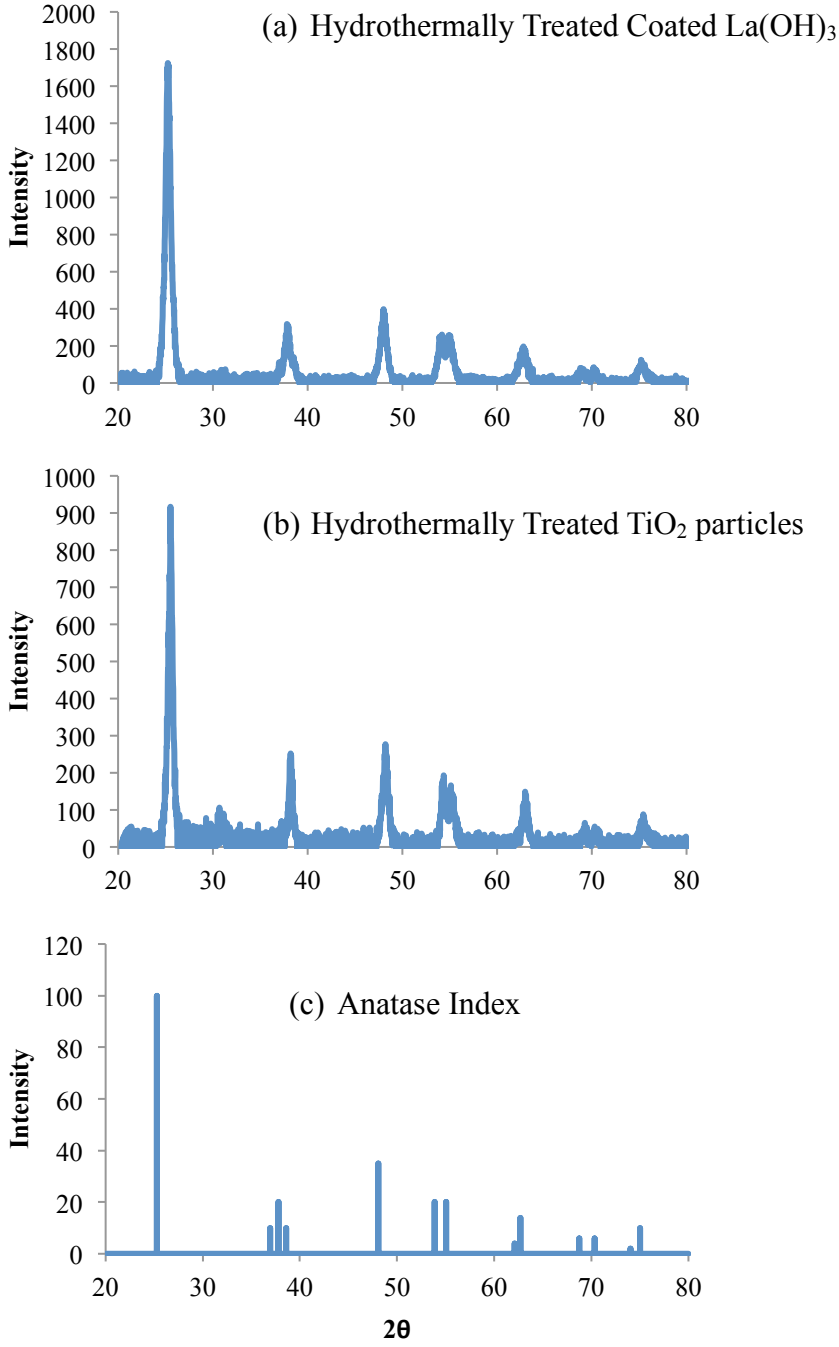

Figure 4-18. XRD pattern of hydrothermally treated TiO_2 and Coated $La(OH)_3$

4.7 Removal in simulated drinking water treatment

As an effort to show the utility of "labeled" TiO_2 nanoparticles, the differential removal of coated and uncoated particles in simulated drinking water treatment was studied. $La(OH)_3$ particles were coated at 90°C using TTIP as a precursor and the coated particles were hydrothermally treated to crystallize the TiO_2 shell. Three tests were performed: one using labeled (TiO_2@$La(OH)_3$) particles; one using unlabeled TiO_2 particles; and a final test using a mixture of both labeled and unlabeled particles. The size and zeta potential of the two different particles are summarized in Table 4-8. The XRD patterns can be found in Figure 4-18. The difference in the size between the labeled and unlabeled particles is thought to be due to the synthesis process. Literature shows that as homogeneous nucleation of the titanium precursor occurs during synthesis of TiO_2 particles, significant aggregation can occur [69]. However the coated particles are stable during the coating process, forming fewer aggregates then the homogeneous nucleation TiO_2 precipitates.

Table 4-8. Hydrodynamic diameter and Zeta Potential of particles used for Jar testing

Sample	D_H (nm)	ZP at pH 7.2 (mev)
TTIP Coated Particles	279.3±5.2	-28.06±5.21
TiO_2 Particles	492.1±7.1	-34.19±3.78

Alum concentration was varied between 0 to 30 mg/L, and turbidity and metals concentrations measured before and after simulated treatment and are shown in Figure 4-19. The pH of the jars after testing was approximately 7.2±0.31. Several of the lanthanum concentrations were below detection limits of 0.5 ppm and indicated by hollow markers illustrating the upper bounds of their concentration. The first test examined the removal of coated particles (Figure 4-19a). Removal of unlabeled TiO_2 nanoparticles was evaluated in a second removal test (Figure 4-19b). These unlabeled particles serve as an example of background titanium particles, possibly occurring as naturally Ti colloids or another class of ENP. In the last test (Figure 4-19c), a

mixture of both labeled and unlabeled particles, serves as a test of the ability to distinguish between the removals of labeled particles and background titanium concentrations.

Examination of the removal rates in Figure 4-19a shows an excellent correlation between Ti and La removal rates, suggesting that the particles are indeed coated and that the Ti and the La are bound together. Turbidity also tracks very well with the removal of the coated particles. The removal of the unlabeled TiO_2 particles occurs at a much greater rate than the coated particles. Ideally, for coated particles to be used as surrogates for unlabeled counterparts, environmental behavior should be the same. An examination of the size shows that the TiO_2 particles are significantly larger than the coated TTIP particles, which was confirmed by hypothesis testing of the raw data; however, this difference in size cannot account for the effect on removal rates. As seen in Table 4-8, the zeta potentials for two particles are slightly different at pH 7.2. Hypothesis testing was performed on the raw data and confirmed this difference to be significant. This slight difference in zeta potential could be from the presence of uncoated areas on the coated particle surface, possibly influencing the destabilization of coated particles in the region where charge neutralization is the primary mechanism of removal. More work is necessary to ensure core-shell materials are removed at the same rate as their unlabeled counterparts.

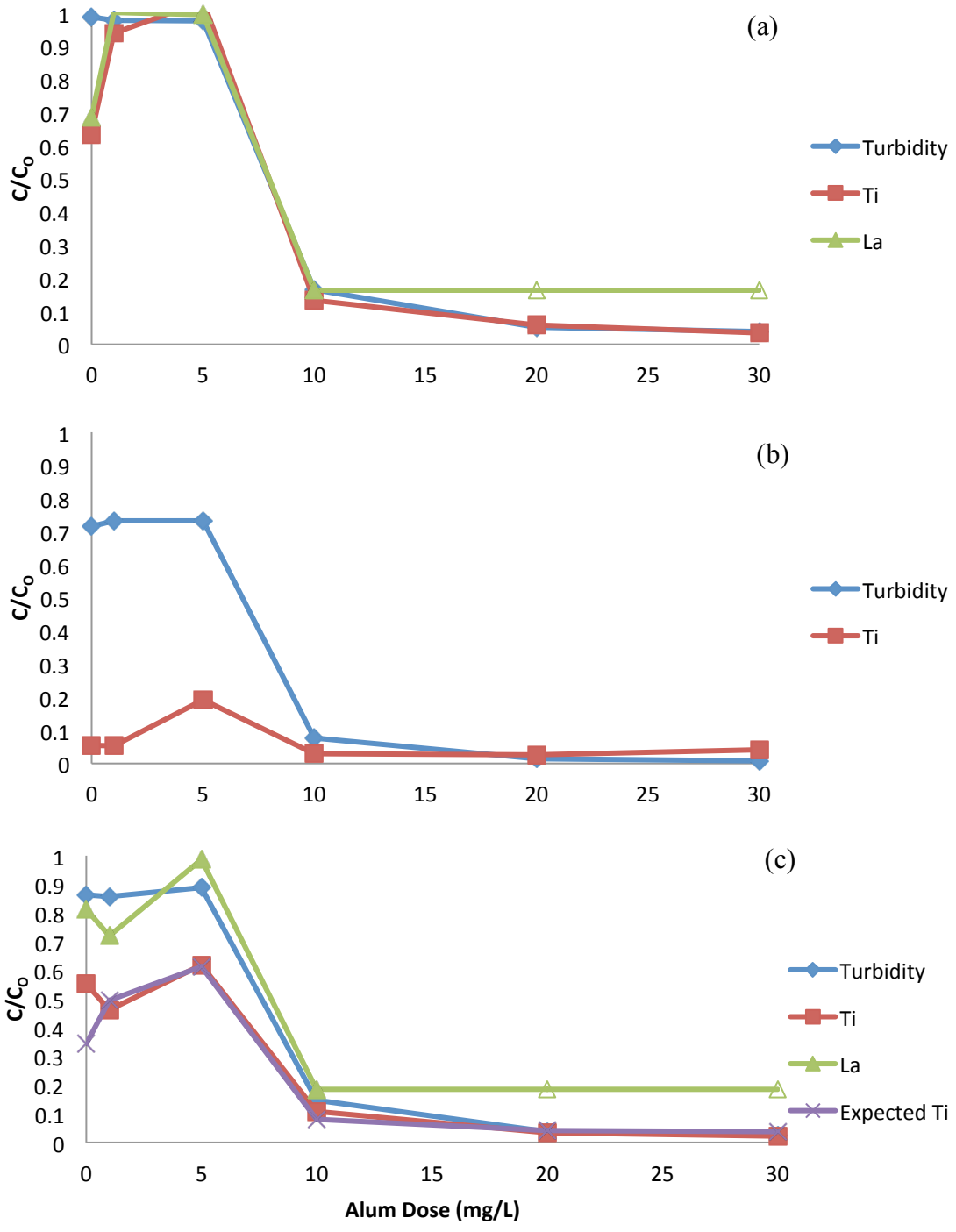

Figure 4-19. Particle removal efficiency during simulated drinking water treatment of coated particles (a), unlabled TiO_2 particles (b), and a mixture of both (c)

The average removal of the Ti:La is 0.585 for the mixed system, indicating the titanium is removed at a greater rate. This result is explained by the greater removal efficiency of the unlabeled TiO_2 particles. Since particles were added at approximately the same concentration, the expected removal of titanium in the mixed system should be the average of the titanium removals between the first two tests. This expected removal is shown on Figure 4-19c, and tracks well with the titanium removal. The ability to quantify the removal of lanthanum against background titanium concentrations allows for the determination of the removal of labeled particles. Without the labeling element, the only data presented in Figure 4-19c is the overall titanium removal, which does not accurately represent the removal of the coated particles. The removal rates found in Figure 4-19a allow the identification of labeled particles against a background of titanium. If a model system was created with naturally occurring Ti colloids, the removal of added titanium nanoparticles could not be characterized. But, this experiment shows that by adding a tracer element, the removal of the traceable particles can be backed out of a system with a high background concentration. Detection of labeled nanoparticles was made possible in this study by the addition of a labeling element to core-shell TiO_2 NPs. Accurate prediction of coated particle removal from a labeling element was demonstrated. Although the ability to detect labeled particles against a background titanium concentration in simulated water treatment has been demonstrated, more work on synthesis techniques is necessary to ensure physio-chemical properties are identical so that core-shell particles are removed at an identical rate and can successfully be used as surrogates in fate and transport studies.

5 Conclusions

This study examined the synthesis of core-shell particles consisting of lanthanum core material with a TiO_2 shell. The project has developed novel methods and procedures along with materials for the further development of traceable metal oxide nanomaterials to enable the study of environmental fate and transport. Along with the development of traceable nanomaterials and the methods to synthesize and characterize them, the ability to detect these particles against background concentrations has been demonstrated. Although further work is necessary to further refine the synthesis and coating of monodisperse lanthanum nanoparticles, this work serves as a proof of concept for the feasibility of the synthesis of such particles and their usefulness in the examination of environmental fate and transport. To our knowledge this is the first time colloids of this La@TiO_2 structure have been synthesized. Examination of synthesis results yielded the following specific conclusions:

- Changes in initial pH do not have an overall effect on the sol-gel coating of lanthanum nanopowder by TiO_2.
- The use of lanthanum as a core material has some drawbacks. Lanthanum materials undergo extremely fast reactions with atmospheric water to form $La(OH)_3$. Lanthanum containing particles and amorphous TiO_2 particles have similar charges at pH values that promote the reaction of titanium alkoxides. Coating must therefore be performed by the slow hydrolysis of titanium precursors via heterogeneous nucleation on the lanthanum nanoparticle surface while taking care to control synthetic conditions so as to avoid homogeneous nucleation of TiO_2 in solution.
- TTIP provides a much more robust coating of titanium dioxide than TBOT, but care must be taken when choosing synthesis conditions so as to not create homogenous nucleates of titanium.
- Reaction of titanium alkoxides on lanthanum particle surfaces can occur without the presence of water, yielding incredibly thin coatings of titanium dioxide. Zeta

potential measurements indicate thin coatings did occur while detection by EDS was not possible because of the small fraction of titanium in the sample.

- Core material choice in the synthesis of core-shell morphology has a profound impact on the coating of the material. Zeta potential curves indicate that $La(OH)_3$ enables a much more complete coverage of TiO_2 than the coating of lanthanum nanopowder. It is hypothesized that the difference in crystal phases of the materials played an important role in the coating of the two materials with TiO_2.
- Hydrothermal treatment of core-shell particles yielded a well-defined crystalline shell without any evidence of a mixed phase system consisting of both La and Ti. Particles size remained roughly unchanged after hydrothermal treatment, while initial calcinations provided powders that were hard to disperse in water yielding large aggregates.
- Titania coated lanthanum hydroxide particles can successfully be detected and quantified against a background titanium concentration. However, the removal of coated $La(OH)_3$ particles and TiO_2 was quite different. Although these particles are suitable for use as a tracer, the fact that they behave differently than their unlabeled counterparts suggests that they are not yet adequate surrogates. Further work needs to be done to ensure the characteristics and behavior (e.g., removal in water treatment) of the two particles are identical to demonstrate usefulness of coated particles as surrogates.

The results of this study provide a framework for the synthesis and demonstration of core-shell particles for use in examining environmental fate and transport. Aggregation state of the starting lanthanum material proved to be problematic in the examination of coating procedures. The study of particle morphology was also challenging due to the inability to achieve stable, monodisperse core particles. Further work using hydrothermal synthesis and homogeneous precipitation of lanthanum materials is needed to provide more monodisperse colloids. Initial work involving the homogenous precipitation of lanthanum particles from $La(NO_3)$ by urea has been performed and yielded large (171 nm

to 294.1 nm) particles with low polydispersities. Further work in this area could yield well-controlled particle morphology. Refinement of the sol-gel coating process is also needed to produce robust coatings of TiO_2 with properties matching those of commercially available materials. The use of TTIP as a precursor provided promising results in this study, but analysis suggested that some TiO_2 particles formed in addition to the coated particles and coatings were incomplete. Further refinement of the process by more tightly controlling the temperature or lowering the concentration of water in solution could eliminate these problems. Future work in this project will investigate the use of other core materials that also have suitable INAA sensitivity such as Au. Primary work in this area has been started and shows promising results for future work. Procedures for synthesizing well-defined gold nanoparticles are well developed, as are some procedures for coating these materials. Analysis of particle size, morphology, and coating yielded varying results between methods, highlighting the need for complementary analysis techniques.

Demonstration of the usefulness of core-shell particles for detection using INAA was not possible because the INAA facility at OSU was down for a long period of repair during the final phase of this work. Future work will evaluate the feasibility of using INAA and ICP-MS to detect low concentrations of labeled particles in environmental matrices containing a background of titanium. Future fate and transport studies using these particles could include, but are not limited to, spike and recovery studies using various environmental matrices (soil, water, sewage sludge, etc.), column studies followed by dissection and analysis of the column using INAA and/or ICP-MS, examination of the partitioning of particles in lab scale waste water treatment such as sequencing batch reactors, and examination of particle uptake by biota using INAA. The work reported here represents substantial progress towards the goal of developing labeled TiO_2 surrogates. TiO_2 particles labeled with La were synthesized and characterized, and their usefulness was demonstrated in proof-of-concept experiments. As such, this work represents a solid foundation and experimental framework for further development of traceable metal oxide nanomaterials. It is anticipated that the further development of

these traceable particles will enable a better understanding of the fate and transport, toxicity, and modeling of metal oxide particles in the environment. The increase in knowledge gained by the development of these particles will enable the development of specific regulations and standards for the use of different nanomaterials.

6 Appendix

Lab synthesized La_2O_3 nanopowder SEM

Initial lab work was done to synthesize La_2O_3 using a procedure from Wang et al. [67]. Particles were highly aggregated and not dispersible by dispersion in water by ultrasonic bath. Upon calcination, particles were left in glass vials for several days prior to XRD analysis. XRD patterns, not shown here, showed complete transformation of the powder into $La(OH)_3$. Because of the initial poor results, and long synthesis times (approximately a week), a lanthanum nanopowder was purchased from Sigma Aldrich and used in initial coating studies.

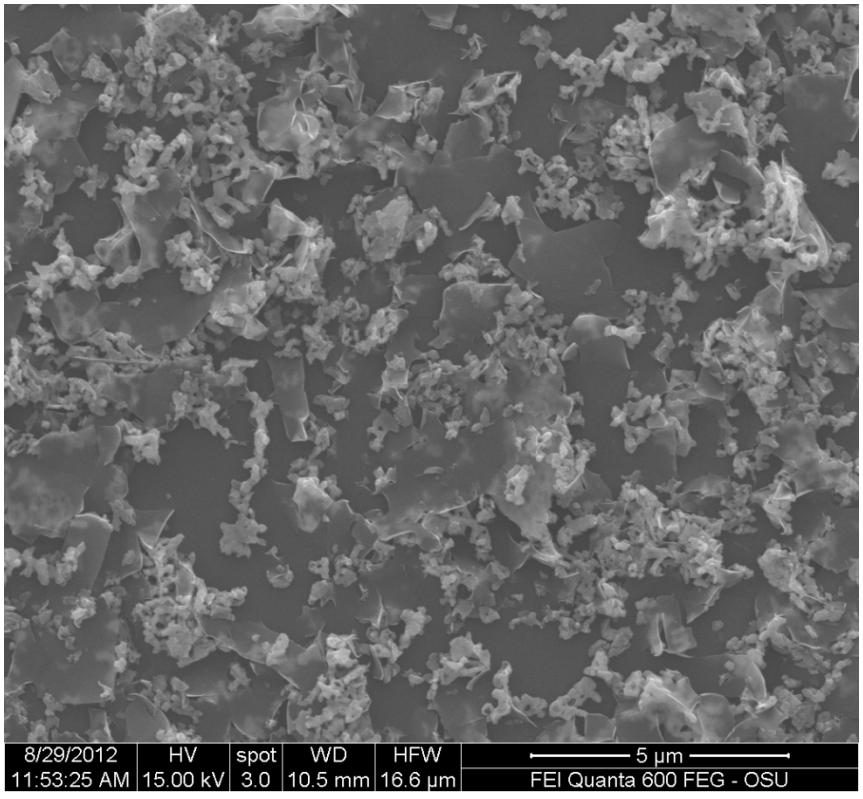

Lanthanum Dissolution Test

To measure the extent of dissolution in acidic pHs, a dispersion of lanthanum nanopowder was adjusted to different pHs and filtered using a 0.02µm syringe filter. Filtrate was analyzed by ICP-AES and compared to the original particle fraction dissolved.

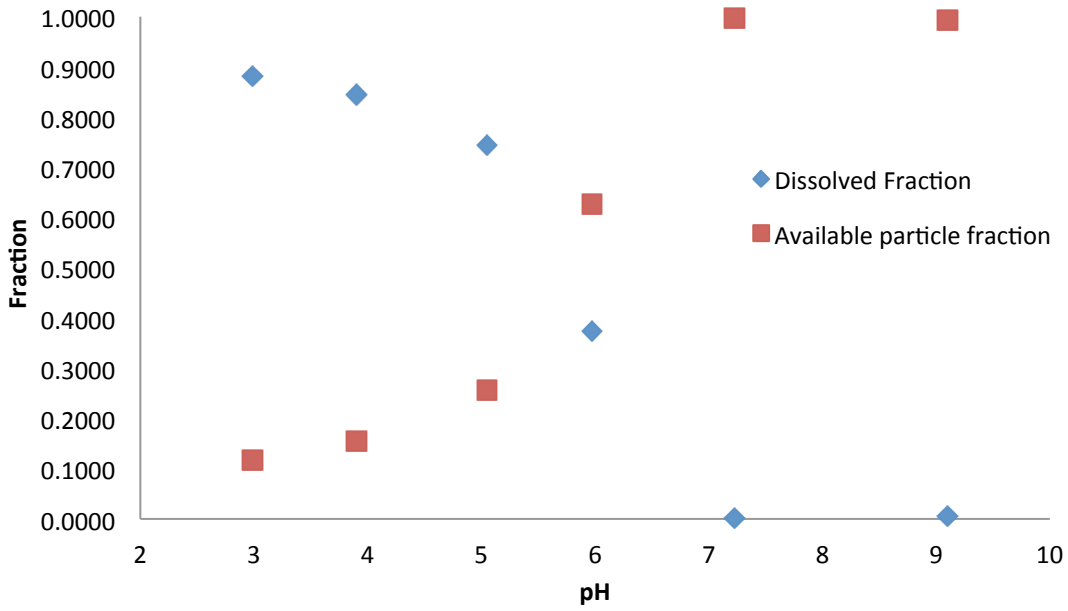

Zeta Potential Curves for coated Lanthanum nanopowder at 0.27M water concentrations

As discussed in 4.2.2, particles were coated at both 0.54M and 0.27M water ratios. The zeta potential curves were very similar between those two water ratios and only the 0.54M water concentration was discussion in the main body of the text. The zeta potential curves for 0.27M water coated particles can be found below.

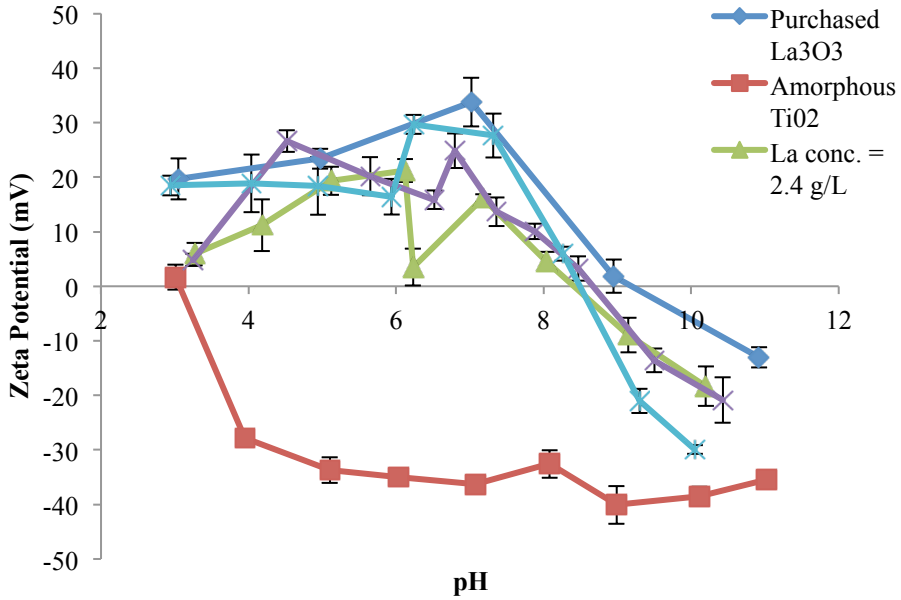

FTIR Spectra for washed $La(OH)_3$ Nanospheres

To ensure $La(OH)_3$ partices were citrate free after rinsing, rinsed particles were dried and analyzed using FTIR, along with sodium citrate. If citrate remained bound to the lanthanum particle surface it could possible interfere with coating of the material. The FTIR curves are seen below.

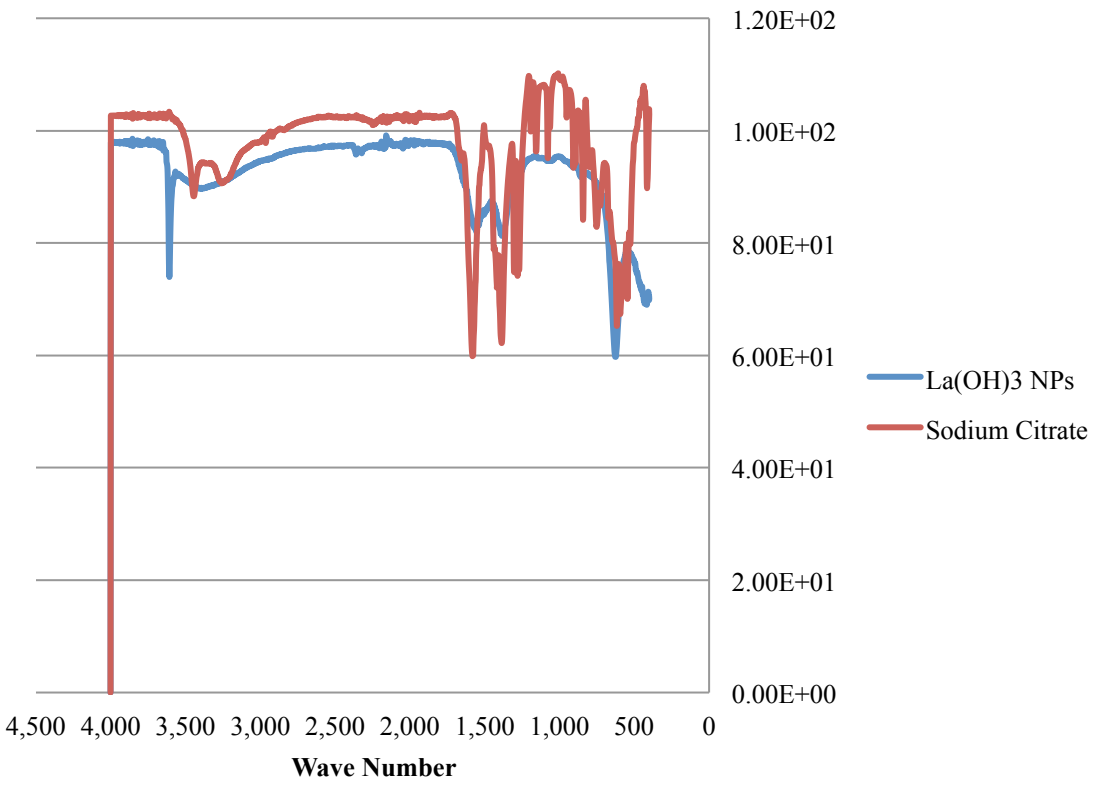

EDS Spectra from coated $La(OH)_3$ 0.54M water using TBOT

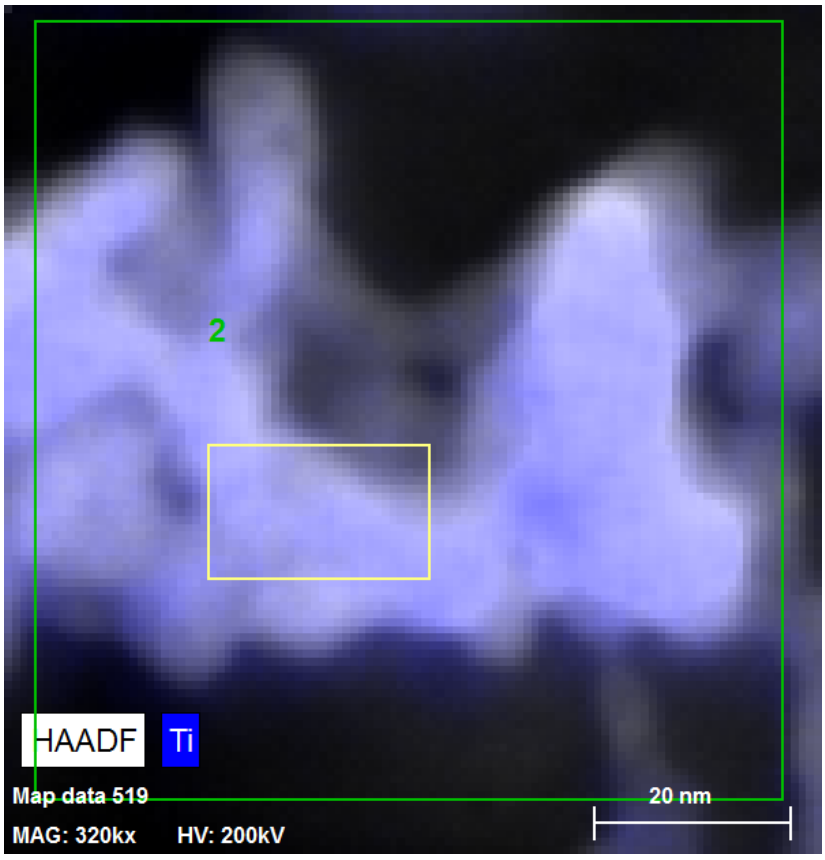

1 Date:6/19/2013 3:25:12 PM
HV:200.0kV Puls th.:4.50kcps

El	AN	Series	unn. C [wt.%]	norm. C [wt.%]	Atom. C [at.%]	Error (1 Sigma) [wt.%]
La	57	L-series	99.60	99.60	98.85	9.99
Ti	22	K-series	0.40	0.40	1.15	0.04
Total:			100.00	100.00	100.00	

EDS Map and spectra of coated $La(OH)_3$ using TTIP

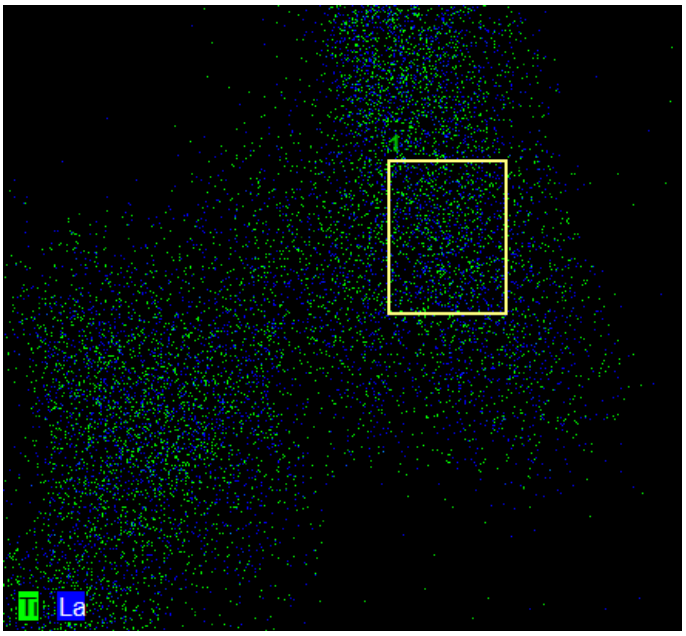

1

Date:8/9/2013 10:53:18 AM HV:200.0kV Puls th.:1.51kcps

El	AN	Series	unn. C [wt.%]	norm. C [wt.%]	Atom. C [at.%]	Error (1 Sigma) [wt.%]
O	8	K-series	24.14	24.14	63.83	0.92
Ti	22	K-series	22.57	22.57	19.94	0.89
La	57	K-series	53.29	53.29	16.23	10.40
		Total:	100.00	100.00	100.00	

Raw linescan counts from dedicated linescan on coated $La(OH)_3$ using TTIP as a precursor

Represented below is the unanalyzed data from the dedicated EDS linescan performed on the $La(OH)_3$ particles coated at 054M water using TTIP as the precursor. The edge of the titanium map occurs at a distance of approximately 21 nm, while the lanthanum maps occurs at approximately 23 nm, indicating a coating of approximately 2 nm.

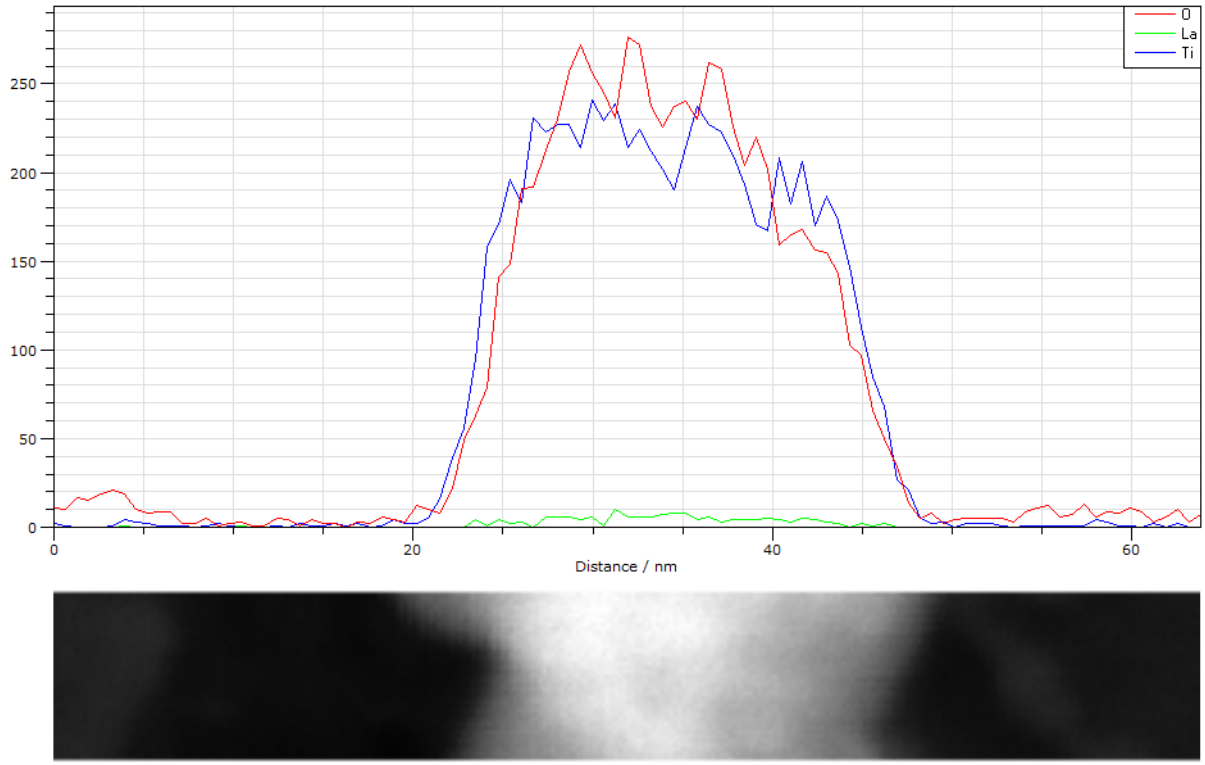

SAXS data from uncoated $La(OH)_3$

Represented below is the SAXS curves from the uncoated La(OH)3 particles. As seen there is a bimodal distribution for the 1 ppm tests, but the peaks all occur at approximately the same radius.

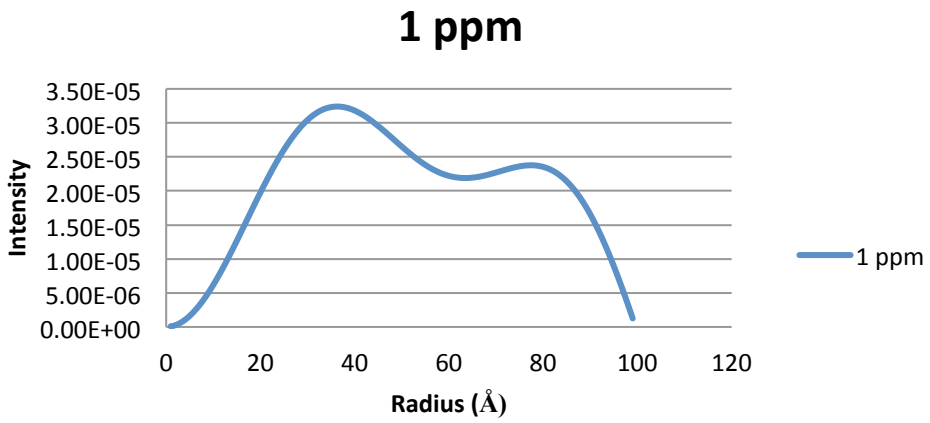

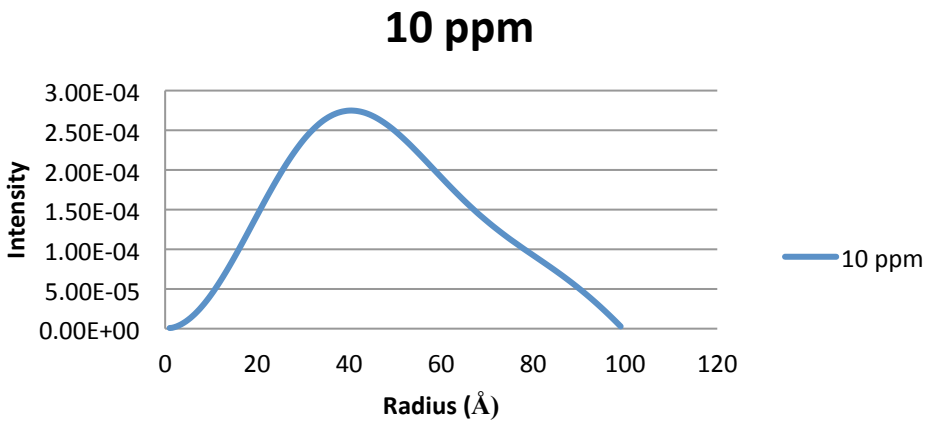

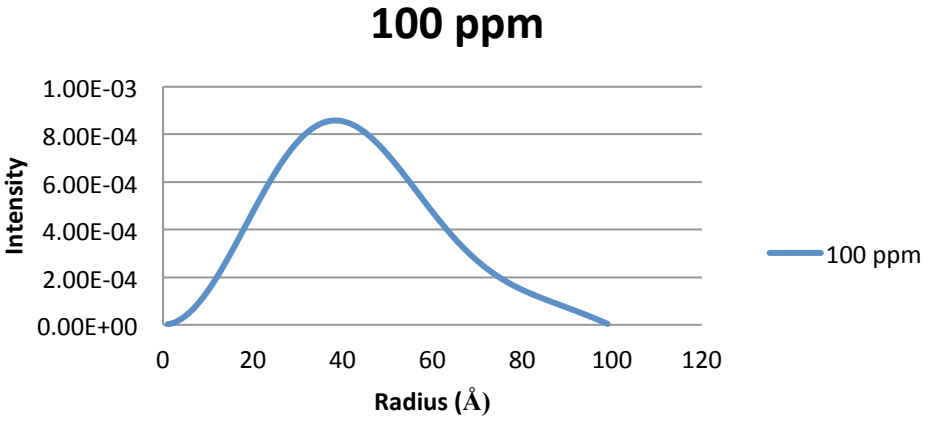

SAXS data from coated $La(OH)_3$ using TBOT

Particles coated with heat using TBOT and 0.54M water were also analyzed by SAXS, the radius was found to be smaller than the original uncoated particles, the curve is represented below.

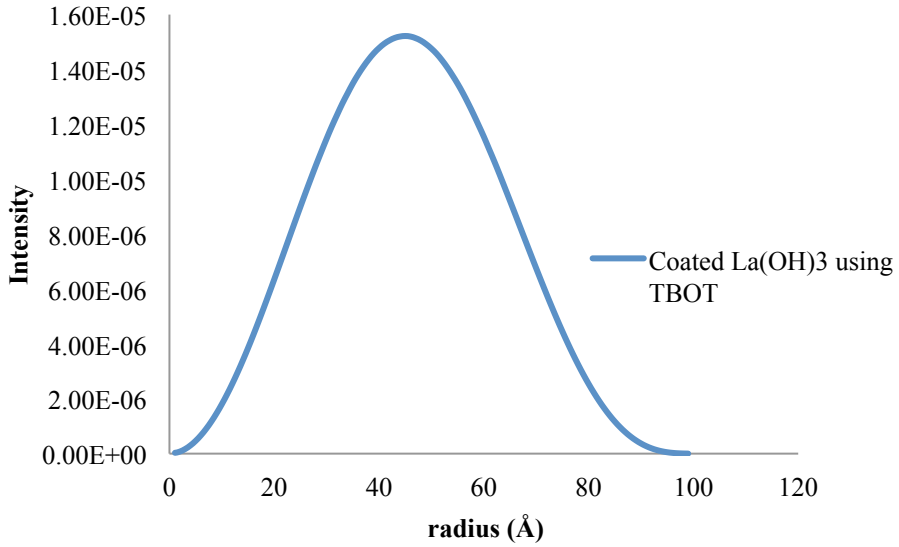

7 Bibliography

1. Zhang, Y., et al., *Stability of commercial metal oxide nanoparticles in water.* Water Research, 2008. **42**(8-9): p. 2204-2212.
2. Biswas, P. and C.Y. Wu, *2005 Critical Review: Nanoparticles and the environment.* Journal of the Air & Waste Management Association, 2005. **55**(6): p. 708-746.
3. Wang, Y.F., P. Westerhoff, and K.D. Hristovski, *Fate and biological effects of silver, titanium dioxide, and C-60 (fullerene) nanomaterials during simulated wastewater treatment processes.* Journal of Hazardous Materials, 2012. **201**: p. 16-22.
4. Robichaud, C.O., et al., *Estimates of Upper Bounds and Trends in Nano-TiO2 Production As a Basis for Exposure Assessment.* Environmental Science & Technology, 2009. **43**(12): p. 4227-4233.
5. Wigginton, N.S., K.L. Haus, and M.F. Hochella, *Aquatic environmental nanoparticles.* Journal of Environmental Monitoring, 2007. **9**(12): p. 1306-1316.
6. Kiser, M.A., et al., *Titanium Nanomaterial Removal and Release from Wastewater Treatment Plants.* Environmental Science & Technology, 2009. **43**(17): p. 6757-6763.
7. Kaegi, R., et al., *Synthetic TiO(2) nanoparticle emission from exterior facades into the aquatic environment.* Environmental Pollution, 2008. **156**(2): p. 233-239.
8. Weir, A., et al., *Titanium Dioxide Nanoparticles in Food and Personal Care Products.* Environmental Science & Technology, 2012. **46**(4): p. 2242-2250.
9. Lomer, M.C.E., R.P.H. Thompson, and J.J. Powell, *Fine and ultrafine particles of the diet: influence on the mucosal immune response and association with Crohn's disease.* Proceedings of the Nutrition Society, 2002. **61**(1): p. 123-130.
10. Madl, A.K. and K.E. Pinkerton, *Health effects of inhaled engineered and incidental nanoparticles.* Critical Reviews in Toxicology, 2009. **39**(8): p. 629-658.
11. Zheng, X., Yi guang Chen, and Rui Wu, *Long-term affects of titaium dioxide nanoparticles on nitrogen and phosphorous removal from wastewater and bacterial community shift in activated sludge.* Environmental Science & Technology, 2011.
12. Federici, G., B.J. Shaw, and R.D. Handy, *Toxicity of titanium dioxide nanoparticles to rainbow trout (Oncorhynchus mykiss): Gill injury, oxidative stress, and other physiological effects.* Aquatic Toxicology, 2007. **84**(4): p. 415-430.
13. Ates, M., et al., *Effects of aqueous suspensions of titanium dioxide nanoparticles on Artemia salina: assessment of nanoparticle aggregation, accumulation, and toxicity.* Environmental Monitoring and Assessment, 2013. **185**(4): p. 3339-3348.
14. Heinlaan, M., et al., *Toxicity of nanosized and bulk ZnO, CuO and TiO2 to bacteria Vibrio fischeri and crustaceans Daphnia magna and Thamnocephalus platyurus.* Chemosphere, 2008. **71**(7): p. 1308-1316.
15. von der Kammer, F., et al., *Analysis of engineered nanomaterials in complex matrices (environment and biota): General considerations and conceptual case studies.* Environmental Toxicology and Chemistry, 2012. **31**(1): p. 32-49.

16. Buffet, P.E., et al., *Fate of isotopically labeled zinc oxide nanoparticles in sediment and effects on two endobenthic species, the clam Scrobicularia plana and the ragworm Hediste diversicolor.* Ecotoxicology and Environmental Safety, 2012. **84**: p. 191-198.
17. Reed, R.B., et al., *Overcoming challenges in analysis of polydisperse metal-containing nanoparticles by single particle inductively coupled plasma mass spectrometry.* Journal of Analytical Atomic Spectrometry, 2012. **27**(7): p. 1093-1100.
18. Tang, B., J.C. Ge, and L.H. Zhuo, *The fabrication of La(OH)(3) nanospheres by a controllable-hydrothermal method with citric acid as a protective agent.* Nanotechnology, 2004. **15**(12): p. 1749-1751.
19. Botta, C., et al., *TiO2-based nanoparticles released in water from commercialized sunscreens in a life-cycle perspective: Structures and quantities.* Environmental Pollution, 2011. **159**(6): p. 1543-1548.
20. McNulty, G.S., *Production of Titanium Dioxide.*
21. Hendren, C.O., et al., *Estimating Production Data for Five Engineered Nanomaterials As a Basis for Exposure Assessment.* Environmental Science & Technology, 2011. **45**(7): p. 2562-2569.
22. Limbach, L.K., et al., *Removal of oxide nanoparticles in a model wastewater treatment plant: Influence of agglomeration and surfactants on clearing efficiency.* Environmental Science & Technology, 2008. **42**(15): p. 5828-5833.
23. Fang, J., et al., *Stability of titania nanoparticles in soil suspensions and transport in saturated homogeneous soil columns.* Environmental Pollution, 2009. **157**(4): p. 1101-1109.
24. Duester, L., et al., *Translocation of Sb and Ti in an undisturbed floodplain soil after application of Sb2O3 and TiO2 nanoparticles to the surface.* Journal of Environmental Monitoring, 2011. **13**(5): p. 1204-1211.
25. Guzman, K.A.D., M.P. Finnegan, and J.F. Banfield, *Influence of surface potential on aggregation and transport of titania nanoparticles.* Environmental Science & Technology, 2006. **40**(24): p. 7688-7693.
26. French, R.A., et al., *Influence of Ionic Strength, pH, and Cation Valence on Aggregation Kinetics of Titanium Dioxide Nanoparticles.* Environmental Science & Technology, 2009. **43**(5): p. 1354-1359.
27. Yang, K., D.H. Lin, and B.S. Xing, *Interactions of Humic Acid with Nanosized Inorganic Oxides.* Langmuir, 2009. **25**(6): p. 3571-3576.
28. Domingos, R.F., N. Tufenkji, and K.J. Wilkinson, *Aggregation of Titanium Dioxide Nanoparticles: Role of a Fulvic Acid.* Environmental Science & Technology, 2009. **43**(5): p. 1282-1286.
29. Westerhoff, P., et al., *Occurrence and removal of titanium at full scale wastewater treatment plants: implications for TiO2 nanomaterials.* Journal of Environmental Monitoring, 2011. **13**(5): p. 1195-1203.
30. Saiers, J.E., J.W. Harvey, and S.E. Mylon, *Surface-water transport of suspended matter through wetland vegetation of the Florida everglades.* Geophysical Research Letters, 2003. **30**(19).

31. Larner, F., et al., *Tracing Bioavailability of ZnO Nanoparticles Using Stable Isotope Labeling.* Environmental Science & Technology, 2012. **46**(21): p. 12137-12145.
32. Ferin, J., G. Oberdorster, and D.P. Penney, *Pulmonary Retention of Ultrafine and Fine Particles in Rats.* American Journal of Respiratory Cell and Molecular Biology, 1992. **6**(5): p. 535-542.
33. Bermudez, E., et al., *Pulmonary responses of mice, rats, and hamsters to subchronic inhalation of ultrafine titanium dioxide particles.* Toxicological Sciences, 2004. **77**(2): p. 347-357.
34. Pagnout, C., et al., *Role of electrostatic interactions in the toxicity of titanium dioxide nanoparticles toward Escherichia coli.* Colloids and Surfaces B-Biointerfaces, 2012. **92**: p. 315-321.
35. Li, Y., et al., *Mechanism of Photogenerated Reactive Oxygen Species and Correlation with the Antibacterial Properties of Engineered Metal-Oxide Nanoparticles.* Acs Nano, 2012. **6**(6): p. 5164-5173.
36. Dunford, R., et al., *Chemical oxidation and DNA damage catalysed by inorganic sunscreen ingredients.* Febs Letters, 1997. **418**(1-2): p. 87-90.
37. Miller, R.J., et al., *TiO2 Nanoparticles Are Phototoxic to Marine Phytoplankton.* Plos One, 2012. **7**(1).
38. Dalai, S., et al., *A comparative cytotoxicity study of TiO2 nanoparticles under light and dark conditions at low exposure concentrations.* Toxicology Research, 2012. **1**(2): p. 116-130.
39. Gottschalk, F., et al., *Modeled Environmental Concentrations of Engineered Nanomaterials (TiO2, ZnO, Ag, CNT, Fullerenes) for Different Regions.* Environmental Science & Technology, 2009. **43**(24): p. 9216-9222.
40. Mueller, N.C. and B. Nowack, *Exposure modeling of engineered nanoparticles in the environment.* Environmental Science & Technology, 2008. **42**(12): p. 4447-4453.
41. Simonet, B.M. and M. Valcarcel, *Monitoring nanoparticles in the environment.* Analytical and Bioanalytical Chemistry, 2009. **393**(1): p. 17-21.
42. Gimbert, L.J., et al., *The influence of sample preparation on observed particle size distributions for contrasting soil suspensions using flow field-flow fractionation.* Environmental Chemistry, 2006. **3**(3): p. 184-191.
43. Nordberg, G. and ScienceDirect (Online service), *Handbook on the toxicology of metals*. 2007, Academic Press: Amsterdam ; Boston. p. xlvii, 975 p.
44. Plathe, K.L., et al., *Using FlFFF and aTEM to determine trace metal-nanoparticle associations in riverbed sediment.* Environmental Chemistry, 2010. **7**(1): p. 82-93.
45. Englert, B.C., *Nanomaterials and the environment: uses, methods and measurement.* Journal of Environmental Monitoring, 2007. **9**(11): p. 1154-1161.
46. Tiede, K., et al., *Detection and characterization of engineered nanoparticles in food and the environment.* Food Additives and Contaminants Part a-Chemistry Analysis Control Exposure & Risk Assessment, 2008. **25**(7): p. 795-821.
47. Domingos, R.F., et al., *Characterizing Manufactured Nanoparticles in the Environment: Multimethod Determination of Particle Sizes.* Environmental Science & Technology, 2009. **43**(19): p. 7277-7284.

48. Heithmar, E.M.a.S.A.P. (2012) *Characterizing Concentrations and Size Distributins of Metal-Containing Nanoparticles in Waste Water*.
49. Pergantis, S.A., T.L. Jones-Lepp, and E.M. Heithmar, *Hydrodynamic Chromatography Online with Single Particle-Inductively Coupled Plasma Mass Spectrometry for Ultratrace Detection of Metal-Containing Nanoparticles.* Analytical Chemistry, 2012. **84**(15): p. 6454-6462.
50. Tiede, K., et al., *A robust size-characterisation methodology for studying nanoparticle behaviour in 'real' environmental samples, using hydrodynamic chromatography coupled to ICP-MS.* Journal of Analytical Atomic Spectrometry, 2009. **24**(7): p. 964-972.
51. Liu, F.K. and G.T. Wei, *Adding sodium dodecylsulfate to the running electrolyte enhances the separation of gold nanoparticles by capillary electrophoresis.* Analytica Chimica Acta, 2004. **510**(1): p. 77-83.
52. Liu, F.K. and F.H. Ko, *Separation and study of the optical properties of silver nanocubes by capillary electrophoresis.* Chemistry Letters, 2004. **33**(7): p. 902-903.
53. Franze, B., I. Strenge, and C. Engelhard, *Single particle inductively coupled plasma mass spectrometry: evaluation of three different pneumatic and piezo-based sample introduction systems for the characterization of silver nanoparticles.* Journal of Analytical Atomic Spectrometry, 2012. **27**(7): p. 1074-1083.
54. Mitrano, D.M., et al., *Silver nanoparticle characterization using single particle ICP-MS (SP-ICP-MS) and asymmetrical flow field flow fractionation ICP-MS (AF4-ICP-MS).* Journal of Analytical Atomic Spectrometry, 2012. **27**(7): p. 1131-1142.
55. Mitrano, D.M., et al., *Detecting nanoparticulate silver using single-particle inductively coupled plasma-mass spectrometry.* Environmental Toxicology and Chemistry, 2012. **31**(1): p. 115-121.
56. Weise, H.P., W. Gorner, and M. Hedrich, *Determination of elements by nuclear analytical methods.* Fresenius Journal of Analytical Chemistry, 2001. **369**(1): p. 8-14.
57. Oughton, D.H., et al., *Neutron activation of engineered nanoparticles as a tool for tracing their environmental fate and uptake in organisms.* Environmental Toxicology and Chemistry, 2008. **27**(9): p. 1883-1887.
58. Glascock, D.M.D. *Overview of Neutron Activation Analysis*. 9/10/13]; Available from: http://archaeometry.missouri.edu/naa_overview.html.
59. Minc, D.L.A.P., OSU Radiation Center. Personal communication. 9/10/2010.
60. Long, Y.L., et al., *Combustion synthesis and stability of nanocrystalline La2O3 via ethanolamine-nitrate process.* Journal of Rare Earths, 2012. **30**(1): p. 48-52.
61. Li, Y.X., X.Z. Zhou, and Z.Q. Wang, *Mechanochemical reaction of lanthanum carbonate with sodium hydroxide and preparation of lanthanum oxide nanoparticle.* Journal of Rare Earths, 2002. **20**(5): p. 411-415.
62. Wang, J.C., et al., *Nano lanthanum oxide preparation by alkalescent ammonium citrate system and its primary biological effect.* Journal of Rare Earths, 2004. **22**(6): p. 913-916.
63. Okumura, M., et al., *Chemical vapor deposition of gold on Al2O3, SiO2, and TiO2 for the oxidation of CO and of H-2.* Catalysis Letters, 1998. **51**(1-2): p. 53-58.
64. Wang, J.J., et al., *Synthesis of TiO2 nanoparticles by premixed stagnation swirl flames.* Proceedings of the Combustion Institute, 2011. **33**: p. 1925-1932.

65. Yue, L. and X.M. Zhang, *Preparation of highly dispersed CeO2/TiO2 core-shell nanoparticles.* Materials Letters, 2008. **62**(21-22): p. 3764-3766.
66. Wu, M.M., et al., *Sol-hydrothermal synthesis and hydrothermally structural evolution of nanocrystal titanium dioxide.* Chemistry of Materials, 2002. **14**(5): p. 1974-1980.
67. Wang, X.G., et al., *A simple sol-gel technique for preparing lanthanum oxide nanopowders.* Materials Letters, 2006. **60**(17-18): p. 2261-2265.
68. Wang, N., Q.F. Zhang, and W. Chen, *Synthesis and magnetic properties of lanthanum orthovanadate nanorods.* Crystal Research and Technology, 2007. **42**(2): p. 138-142.
69. Vorkapic, D. and T. Matsoukas, *Effect of temperature and alcohols in the preparation of titania nanoparticles from alkoxides.* Journal of the American Ceramic Society, 1998. **81**(11): p. 2815-2820.
70. Ocana, M., W.P. Hsu, and E. Matijevic, *Preparation and Properties of Uniform-Coated Colloidal Particles .6. Titania on Zinc-Oxide.* Langmuir, 1991. **7**(12): p. 2911-2916.
71. Pierre, A.C., *Introduction to Sol-Gel Processing*. 1998.
72. Xu, A.W., Y. Gao, and H.Q. Liu, *The preparation, characterization, and their photocatalytic activities of rare-earth-doped TiO2 nanoparticles.* Journal of Catalysis, 2002. **207**(2): p. 151-157.
73. Stengl, V., S. Bakardjieva, and N. Murafa, *Preparation and photocatalytic activity of rare earth doped TiO2 nanoparticles.* Materials Chemistry and Physics, 2009. **114**(1): p. 217-226.
74. Sibu, C.P., et al., *Structural modifications and associated properties of lanthanum oxide doped sol-gel nanosized titanium oxide.* Chemistry of Materials, 2002. **14**(7): p. 2876-2881.
75. Sartori, A., et al., *Preparation of tetrapod-like ZnO/TiO2 core-shell nanostructures as photocatalytic powder.* Crystal Research and Technology, 2011. **46**(8): p. 885-890.
76. Liao, M.H., C.H. Hsu, and D.H. Chen, *Preparation and properties of amorphous titania-coated zinc oxide nanoparticles.* Journal of Solid State Chemistry, 2006. **179**(7): p. 2020-2026.
77. Wu, X.F., et al., *Synthesis of Core-Shell Au@TiO2 Nanoparticles with Truncated Wedge-Shaped Morphology and Their Photocatalytic Properties.* Langmuir, 2009. **25**(11): p. 6438-6447.
78. Du, J., et al., *Facile synthesis of Au@TiO2 core-shell hollow spheres for dye-sensitized solar cells with remarkably improved efficiency.* Energy & Environmental Science, 2012. **5**(5): p. 6914-6918.
79. Caruso, R.A. and M. Antonietti, *Sol-gel nanocoating: An approach to the preparation of structured materials.* Chemistry of Materials, 2001. **13**(10): p. 3272-3282.
80. Demirors, A.F., A. van Blaaderen, and A. Imhof, *A General Method to Coat Colloidal Particles with Titania.* Langmuir, 2010. **26**(12): p. 9297-9303.
81. Seh, Z.W., et al., *Anisotropic Growth of Titania onto Various Gold Nanostructures: Synthesis, Theoretical Understanding, and Optimization for Catalysis.* Angewandte Chemie-International Edition, 2011. **50**(43): p. 10140-10143.

82. Li, J. and H.C. Zeng, *Nanoreactors - Size tuning, functionalization, and reactivation of Au in TiO2 nanoreactors.* Angewandte Chemie-International Edition, 2005. **44**(28): p. 4342-4345.
83. Sheng, J., et al., *Surfactant-assisted synthesis and characterization of lanthanum oxide nanostructures.* Journal of Materials Science, 2007. **42**(23): p. 9565-9571.
84. Stankus, D.P., et al., *Interactions between Natural Organic Matter and Gold Nanoparticles Stabilized with Different Organic Capping Agents.* Environmental Science & Technology, 2011. **45**(8): p. 3238-3244.
85. Barnett, C.E., *Some Applications of Wave-length Turbidimetry in the Infrared.* J. Phys. Chem, 1941. **46**(1): p. 69-75.
86. Shtykova, E.V., et al., *Structure and properties of iron oxide nanoparticles encapsulated by phospholipids with poly(ethylene glycol) tails.* Journal of Physical Chemistry C, 2007. **111**(49): p. 18078-18086.
87. Scolan, E. and C. Sanchez, *Synthesis and characterization of surface-protected nanocrystalline titania particles.* Chemistry of Materials, 1998. **10**(10): p. 3217-3223.
88. Zhou, D.X., S.W. Bennett, and A.A. Keller, *Increased Mobility of Metal Oxide Nanoparticles Due to Photo and Thermal Induced Disagglomeration.* Plos One, 2012. **7**(5).
89. Suttiponparnit, K., et al., *Role of Surface Area, Primary Particle Size, and Crystal Phase on Titanium Dioxide Nanoparticle Dispersion Properties.* Nanoscale Research Letters, 2011. **6**.
90. Salavati-Niasari, M., G. Hosseinzadeh, and O. Amiri, *Synthesis of Monodisperse Lanthanum Hydroxide Nanoparticles and Nanorods by Sonochemical Method.* Journal of Cluster Science, 2012. **23**(2): p. 459-468.
91. Hirakawa, T. and P.V. Kamat, *Charge separation and catalytic activity of Ag@TiO2 core-shell composite clusters under UV-irradiation.* Journal of the American Chemical Society, 2005. **127**(11): p. 3928-3934.
92. Kim, K.Y. and Y.H. Yun, *Surface modification of oxide phosphors using nano powders.* Journal of Ceramic Processing Research, 2007. **8**(6): p. 421-426.
93. Fleming, P., et al., *The Rapid Formation of La(OH)(3) from La2O3 Powders on Exposureto Water Vapor.* Journal of the American Ceramic Society, 2010. **93**(4): p. 1187-1194.
94. Hintz, W., et al., *Surface-modification of Silica-particles by nano-sc aled Titania-particles via Sol-Gel-Process.*
95. Chanaud, P., et al., *Study of Lanthanum-Based Colloidal Sols Formation.* Journal of Materials Science, 1994. **29**(16): p. 4244-4251.
96. Wang, Z.L., *Transmission electron microscopy of shape-controlled nanocrystals and their assemblies.* Journal of Physical Chemistry B, 2000. **104**(6): p. 1153-1175.
97. Stumm, W.a.J.J.M., ed. *Aquatic Chemistry: Chemical Equilibria and Rates in Natural Wateres*. 3rd ed. 1996, John Wiley & Sons, Inc.: New York, NY.

98. Stockinger, A.J., *Optimizing Lanthanum (III) hydroxide by varying drying methods to maximize surface area to adsorb arsenic in water*. 2007, University of Nevada, Reno: Reno. p. 75.
99. Dong, J., et al., *Effect of Triton X-100 on the stability of aqueous dispersions of copper phthalocyanine pigment nanoparticles.* Journal of Colloid and Interface Science, 2011. **362**(1): p. 33-41.
100. Prasai, B., et al., *Properties of amorphous and crystalline titanium dioxide from first principles.* Journal of Materials Science, 2012. **47**(21): p. 7515-7521.